

Article

Cold Coastal City Neighborhood Morphology Design Method Based on Multi-Objective Optimization Simulation Analysis

Sheng Xu ¹, Peisheng Zhu ^{1,*}, Fei Guo ^{1,*} , Duoduo Yan ¹, Shiyu Miao ¹, Hongchi Zhang ¹ , Jing Dong ¹ 
and Xianchao Fan ²

¹ College of Architecture and Art, Dalian University of Technology, Dalian 116024, China; xusheng@mail.dlut.edu.cn (S.X.); miaoshiyu@mail.dlut.edu.cn (S.M.)

² China Construction Industrial & Energy Engineering Group Co., Ltd., Nanjing 210000, China

* Correspondence: jz-acoustics@dlut.edu.cn (P.Z.); guofei@dlut.edu.cn (F.G.)

Abstract: In the context of global warming and the frequent occurrence of extreme weather, coastal cities are more susceptible to the heat island effect and localized microclimate problems due to the significant influence of the oceanic climate. This study proposes a computer-driven simulation optimization method based on a multi-objective optimization algorithm, combined with tools such as Grasshopper, Ladybug, Honeybee and Wallacei, to provide scientific optimization decision intervals for morphology control and evaluation factors at the initial stage of coastal city block design. The effectiveness of this optimization strategy is verified through empirical research on typical coastal neighborhoods in Dalian. The results show that the strategy derived from the multi-objective optimization-based evaluation significantly improves the wind environment and thermal comfort of Dalian neighborhoods in winter and summer: the optimization reduced the average wind speed inside the block by 0.47 m/s and increased the UTCI by 0.48 °C in winter, and it increased the wind speed to 1.5 m/s and decreased the UTCI by 0.59 °C in summer. This study shows that the use of simulation assessment and multi-objective optimization technology to adjust the block form of coastal cities can effectively improve the seasonal wind and heat environment and provide a scientific basis for the design and renewal of coastal cities.



Citation: Xu, S.; Zhu, P.; Guo, F.; Yan, D.; Miao, S.; Zhang, H.; Dong, J.; Fan, X. Cold Coastal City Neighborhood Morphology Design Method Based on Multi-Objective Optimization Simulation Analysis. *Buildings* **2024**, *14*, 3176. <https://doi.org/10.3390/buildings14103176>

Academic Editor: Rafik Belarbi

Received: 31 August 2024

Revised: 28 September 2024

Accepted: 29 September 2024

Published: 5 October 2024



Copyright: © 2024 by the authors. Licensee MDPI, Basel, Switzerland. This article is an open access article distributed under the terms and conditions of the Creative Commons Attribution (CC BY) license (<https://creativecommons.org/licenses/by/4.0/>).

Keywords: multi-objective optimization; cold coastal areas; microclimate; urban block shape design

1. Introduction

As urbanization accelerates and the size of the urban population expands, the demand for urban infrastructure and land expansion is surging, and people's transformation of natural resources and the environment is in turn having a profound impact on the urban living environment [1]. As a result, global warming, the urban heat island effect, and climate extremes are increasing. In response to these challenges, inhabitants of different climate regions have taken various measures, including supporting policies to promote sustainable development, alongside developing new energy vehicles and advancing green building technologies, as part of broader scientific and technological innovation [2–7]. It is hoped that these measures will alleviate the pressure on the city's ecological environment. However, the city, as a complex design system, must carefully consider its capacity and related indicators at the early stages of planning in order to create a comfortable living environment for its inhabitants while maintaining a reasonable rate of urban growth. The layout of buildings and city blocks is one of the key factors affecting the local climate [8]. Well-designed urban neighborhoods not only enhance urban resilience and effectively respond to regional climatic challenges (e.g., strong winds, low temperatures, hot sun, heavy rainfall) but also provide more comfortable living environments for residents [9–11]. Therefore, a deeper understanding of the relationship between the urban neighborhood form and the microclimate can help to more accurately predict the impacts of design

solutions on the future climate, thereby facilitating a more responsible decision-making process [12,13].

1.1. Wind Environment

Ocean winds are an important factor affecting the thermal environment and thermal comfort in coastal urban neighborhoods, and the relationship with the urban form is extremely complex [14,15]. Air movement in cities is not only influenced by the geometry and layout of buildings but is also closely related to the acceleration, dissipation or turbulence generated by the crisscrossing of building clusters [16]. Properly understanding and controlling these interactions is critical to improving the urban wind environment and enhancing outdoor thermal comfort [17,18].

The wind environment in coastal cities is more complex due to the influence of ocean winds, and the interaction between the morphology of buildings and the urban layout with the wind flow affects the overall living environment and thermal comfort of the city [19]. Although there are many research cases related to the wind environment in coastal cities [13,20,21], most of them focus on warm climate regions, and the number and depth of research cases on coastal cities in cold or variable climates are still insufficient. If wind environment analysis can be introduced early in the design of a coastal city and data can be used to optimize the shape, orientation and height of buildings, adverse wind effects can be reduced and the comfort of pedestrians and residents can be enhanced. It is therefore crucial to understand these interactions prior to design and construction.

By incorporating wind environment analysis into the design process, designers can quickly adjust the shape, orientation and layout of buildings to actively regulate the wind flow, enhance the passive ventilation in urban spaces and improve indoor and outdoor thermal comfort [22]. This wind environment-centered approach to urban planning and design can create a healthier and more livable environment for urban residents. Moreover, with the continuous development of computer technology and simulation software, there are now studies and related software that can more accurately simulate and assess the interaction between the wind environment and urban space [23–25]. These studies and simulation and analysis software can identify and resolve potential problems in advance of the design phase, ensuring a more scientific approach to the environmental performance of the urban form and building design.

1.2. Thermal Comfort

The urban thermal environment and thermal comfort are not only affected by ocean wind factors but also closely related to urban form design. The layout and form of buildings, as well as the design of urban spaces, directly affect the distribution of solar radiation and the accumulation and emission of heat, and these changes in the thermal environment in turn affect the thermal comfort experience of residents. Currently, research on thermal environment evaluation systems and indicators has reached a high level of maturity, with key methods such as Predicted Mean Vote (PMV) [26], Physiological Equivalent Temperature (PET) [27,28], and Universal Thermal Climate Index (UTC) being widely recognized and applied in various studies to assess thermal comfort under different environmental conditions [29,30]. The accuracy of regional thermal environment assessments varies depending on the climatic region and the use of different evaluation metrics [31–33]. In urban design, different building forms and spatial configurations can affect the accumulation or dissipation of heat. If designers are able to analyze thermal comfort evaluation indexes at the early stage of the design process, they can more accurately assess the actual impact of such measures on thermal comfort and thus optimize the building layout and material selection to improve thermal comfort.

As computer technology advances, new software for thermal environment evaluation is continuously being developed, including tools like Rayman for calculating thermal comfort [26], ENVI-MET for simulating thermal environments [34], and the most recent UTCI calculation module created for the Rhino-Grasshopper platform [35,36]. Applying these

tools across various climate zones and tailored to specific target characteristics enhances the accuracy and overall quality of thermal environment assessments, paving the way for more precise evaluations [37,38]. The UTCI Calculation plug-in on the Rhino-Grasshopper platform lets designers import EWP climate data [39], calculate thermal comfort for different design scenarios, and optimize the building layout, materials, and shading to improve the city's thermal environment performance during planning; it is now widely used in urban design studies [40,41].

1.3. Evaluating Design Methodologies

In summary, most of the studies on the wind and thermal environments of coastal cities focus on warm areas, and they often only assess the wind or thermal environments individually. In addition, there is a lack of multi-objective optimization techniques in the software simulation of urban wind and thermal environments, especially for the simulation of wind and thermal environments in coastal cities in cold regions. In this context, this paper presents a multi-objective optimization method for urban form simulation based on the Grasshopper for Rhino platform, using Dalian as a case study. The method simulates and optimizes the layout of typical blocks in the city to derive the best distribution scheme. Additionally, this paper analyzes the characteristics of this optimal scheme to develop strategies for improving similar blocks. Ultimately, the method aims to enhance the wind-heat environment in coastal city blocks located in cold regions. The main objectives of this study are as follows:

- a. Explore the effects of different design elements on urban wind and thermal environments by controlling design variables and building an ideal model combination.
- b. Using a multi-objective optimization tool to explore the optimal equilibrium configuration of the coastal urban form in cold regions and initializing a preliminary optimal design strategy based on the optimal solution characteristics.
- c. Based on the strategy derived from multi-objective optimization, the real neighborhood case of Dalian City is optimized and the results before and after the optimization are compared in order to verify the effectiveness of the optimization strategy, so as to assess the potential of the optimal design of urban simulation proposed in this study.

2. Methodology and Tools

2.1. Overview of the Study

This study is mainly divided into two phases: the first phase entails the determination of the decision interval of the optimization strategy of the ideal model simulation through the establishment of an ideal model to explore the main influencing factors affecting the wind-heat environment in urban neighborhoods and the use of multi-objective optimization and genetic algorithm optimization to determine the best optimization strategy. The second stage involves the validation of the optimization results for the real case, where the optimization strategy derived from the ideal model optimization is used to optimize a real neighborhood case in Dalian, and the UTCI and wind environment before and after the optimization are compared using the simulation and evaluation process in the first stage, and the performance potential of the simulation and optimization methodology is evaluated based on the comparison results (Figure 1).

In this study, Rhino and Grasshopper are used as parametric simulation platforms. Rhino has powerful 3D modeling capability, which can model different building forms, and it is extremely convenient to modify the model in real time. Grasshopper has the capability of generating and adjusting the scenario model, and it can achieve the scenario performance indexes through scripting language. Grasshopper has the ability to generate and adjust the program model, and it can realize the calculation of program performance indexes through script language. It also has the characteristics of programming, strong adaptability and good scalability [42]. In addition, Grasshopper supports multi-objective optimization algorithms and uses the Optimization Calculator plug-in to meet the needs of the optimal design of the solution. For the calculation part, the Ladybug Tools performance analysis

plug-in is used. Ladybug Tools provides a series of components for climate analysis, energy simulation, sunlight analysis, air flow analysis and other sustainable design aspects, such as Ladybug, Honeybee, Butterfly, Dragonfly, etc., which are respectively used for the simulation of different parts of the simulation for simulation calculations.

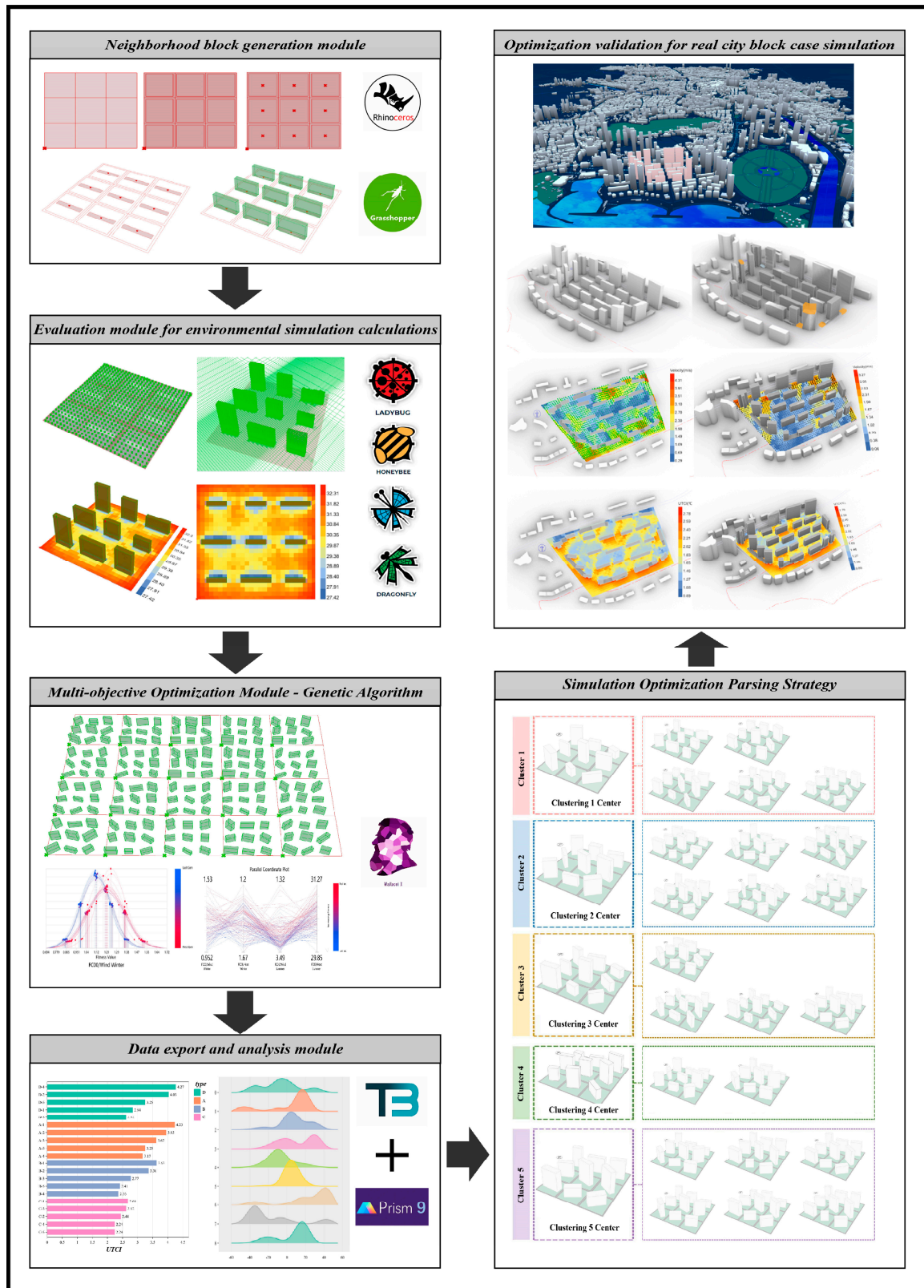


Figure 1. Research flowchart.

2.2. Ideal Model Boundary Conditions and Morphology Generation Module Settings

The first step in the simulation study involves setting up the base model. Since this study mainly focuses on the influence of the building form on the wind–heat environment and thermal comfort, the influence of neighboring buildings is not taken into account in the process of setting up the ideal model. Typical city block sizes range from 200 to 500 m. Due to the high economic value of the blocks in the coastal area, the block size is small and the plot ratio is high, and due to the limitation of the simulation equipment, the simulation takes the ideal block size as the middle value of 200~500 m, which is set to be 270×270 m in order to facilitate the control of the building size, morphology, and other variables. The parcels are divided into 3×3 grids to generate 9 small parcels of 90×90 m. The small plots are offset inward by 5 m as the red line of the road inside the ideal neighborhood, and then the red line of the road is offset inward by another 5 m to form the red line of the building, i.e., the site area of the building on each small unit is 70×70 m and the width of the road is 10 m, which generates a total of 9 small units with the dimensions of 70×70 m. The above boundary condition settings can provide a threshold adjustment space for the later multi-objective optimization generation (Figure 2). Other building layout constraints are set based on relevant codes, mainly fire prevention requirements, sunlight requirements, setback requirements, and minimum building spacing requirements (Table 1).

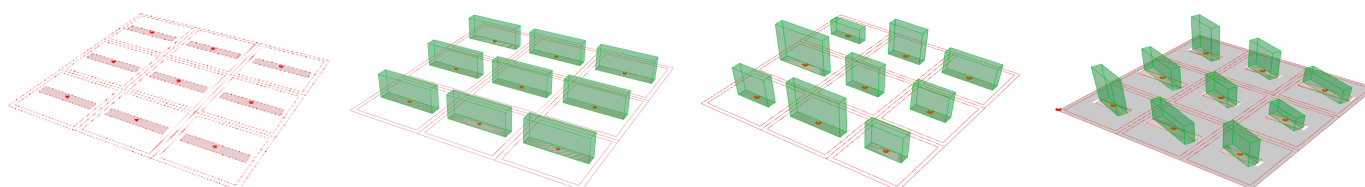


Figure 2. Three-dimensional schematic of the boundary condition setting and variable control for the ideal model.

Table 1. Preset constraint conditions.

Serial Number	Restricted Subjects	Restrictive Condition	Source of Constraints
1	Fire interval	A fire separation of more than 13 m should be maintained between the main bodies of the upper floors.	Fire Code for Building Design
2	Sunlight requirements	Calculation starting point: the position of the exterior wall at a height of 0.9 m from the interior floor. Winter: south residential sunshine duration ≥ 3 h, south public building sunshine duration ≥ 2 h.	Code for Planning and Design of Urban Residential Areas
3	Building line	Multi-story building setbacks of at least 5 m. Tall building setbacks of at least 10 m.	
4	Minimum building spacing	Residential high-rise buildings parallel minimum spacing of not less than 35 m. Minimum parallel spacing of non-residential high-rise buildings of not less than 18 m.	Provisions of Dalian Municipality on the Treatment of Urban Building Spacing and Sunlight Blocking

In terms of the neighborhood layout, the location of the datum point of each small unit site remains unchanged, and the differentiation of individual buildings is mainly reflected in the building plan, floor height and orientation. Therefore, in the optimized control experiments in this simulation study, the range is mainly limited to these 3 main parameters. The building plan is determined by the length and width. The range of the length is 40 m, 50 m, 60 m, 70 m, and the specific operation is to set the gene value of the Gene Pool to 4, 5, 6, 7 by Grasshopper, multiply it by 10 and then divide it by 2 to obtain the Domain start, multiply it by -1 to obtain the Domain end, and then utilize the Construct Domain battery to obtain the length. The range of the width is 10 m, 15 m, 20 m, 25 m,

achieved by setting the gene value of the Gene Pool to 2, 3, 4, 5, and multiplying by 5 to obtain the width range.

The building height is mainly determined by the number of building floors. In this study, the number of building floors varies between 10 and 26, so set the gene in the Gene Pool to take the value range of 10–26, and then multiply the gene value by 3 to obtain the height of the building, which varies between 30 and 78, a total of 17 variables. The floor height and length of each single building are selected within the above variables, and a neighborhood building cluster with different forms of each single building can be generated from this. The range of the building orientation is between -45° south west and 45° south east, and the range of the gene values in the Gene Pool is set to be between -9 and 9 . Then, the gene values are multiplied by 5 to obtain the 19 variables for the building orientation. The orientation of each individual building is selected within the above variables, thus generating a cluster of neighborhood buildings with different orientations of each individual building (Figure 2).

The architectural layout pattern of urban neighborhoods is complex and varied, but most of them are evolved from rows and columns, point-type and enclosure-type. Plate-type buildings are arranged in regular rows, which can strive for the best orientation for the building and is conducive to ventilation, and this is the most common spatial pattern in the layout. Point-type buildings, also known as tower-type buildings, refer to buildings arranged with a common staircase or elevator as the core, and the number of building floors is usually high. The east–west-oriented building rooms of the enclosing buildings are poorly oriented, which is unfavorable to the natural ventilation, and there is no good sunshine, but the space formed is closed and the sense of belonging is strong (Figure 3).

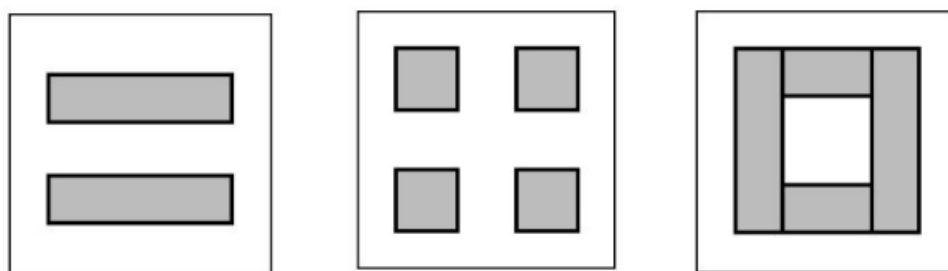


Figure 3. Top view of a typical neighborhood building plan layout.

Based on the above characteristics of the urban block layout, this study sets up 20 groups of controlled experiments by changing the single variable factors, and it conducts thermal comfort simulations for the slab layout, point layout, and courtyard layout in the single variable as much as possible. Setting the specific parameters, using control variables described in Table 2, generates the building layout in Figure 4.

Table 2. Experimental control group parameter settings.

Controlling Morphological Factors	Realm	Remarks
Building type	A, B, C, D	A, B: Panel, C: Point, D: Enclosure
Building height	A: 24 m; B: 54 m C: 54 m; D: 21 m or 16.8 m	A and B are building height control experiments; the height of D varies with the number of floors, with each floor having a height of 4.2 m.
Building plan	A,B: 60×15 m; C: 40×40 m; D: 60×15 m and 35×10 m;	The simulation of D is classified as fully enclosed, semi-enclosed, and fully open.
Building orientation	45° south–east– 45° north–east $^\circ$	See Figure 4 for details.

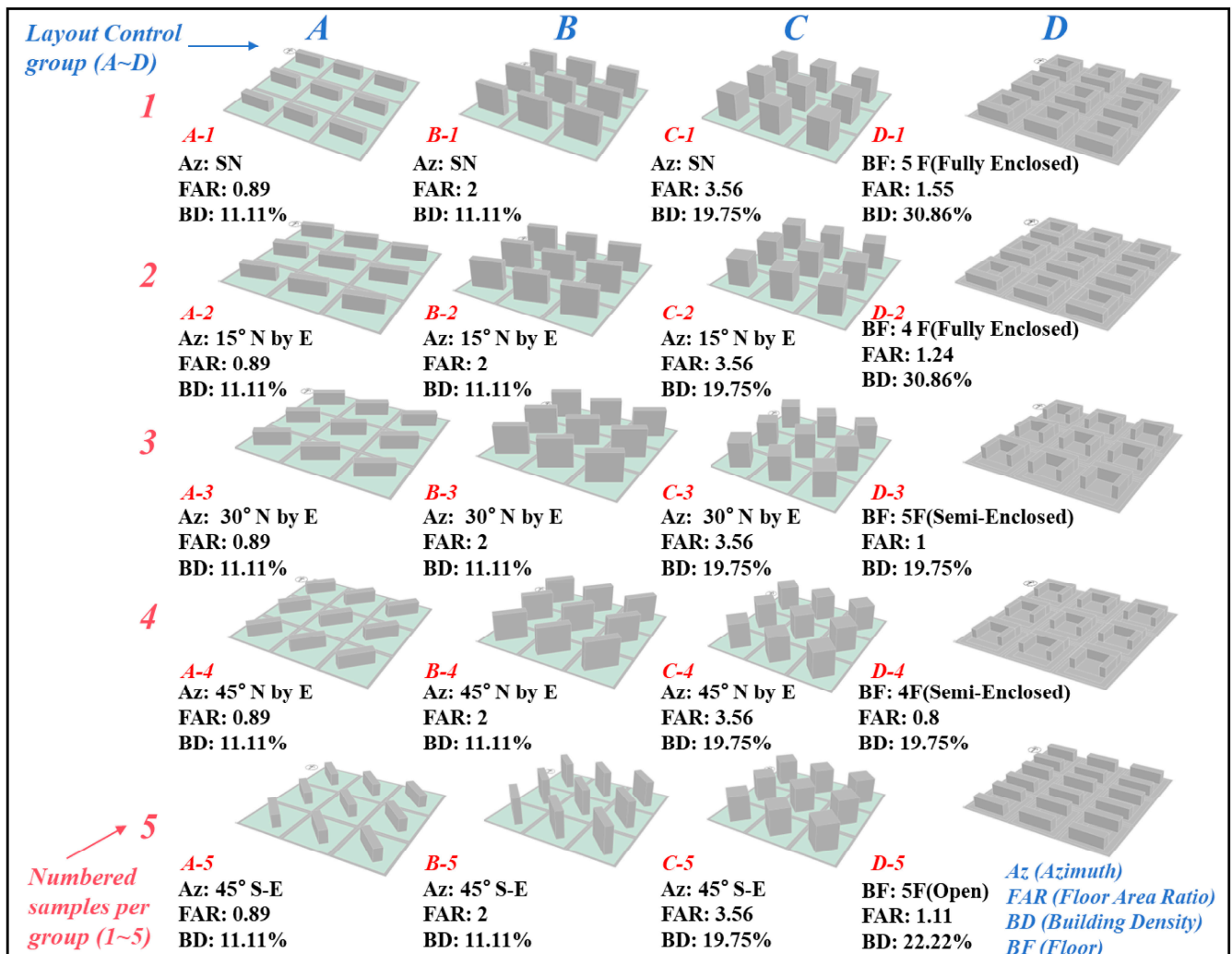


Figure 4. Ideal model for the experimental control group.

2.3. Ideal Model Simulation Conditions Parameter Setting and Optimization Tools

2.3.1. Parameterization of Microclimate Conditions

This study utilizes the Dragonfly (DF) plug-in to call the data interface of Urban Weather Generator (UWG), a plug-in developed by the MIT Building Technology Research Team to support research in the fields of urban planning and climate change, which simulates the microclimate inside city streets [43]. Meteorological parameters use EPW meteorological data developed by the U.S. Department of Energy, including hourly meteorological data for a year, including the outdoor temperature, humidity, wind speed, wind direction, radiation and other parameters. The UWG tool is used for outdoor thermal comfort simulations at the neighborhood scale due to the large errors in the direct use of EPW meteorological data, while the UWG tool in the DF plug-in improves the accuracy of the meteorological data. The simulation time and date are set as 8:00–16:00 on 22 January, the coldest day of a typical winter in the coastal area. In addition, in order to be closer to the real coastal wind environment conditions, the simulation wind environment parameters are set as a dynamic wind direction and wind speed.

The specific simulation steps can be divided into four parts: building form setting, model creation, city parameter setting and simulation running. First, import the neighborhood building model through the DF building from Solid operator, set the floor height to 3 m and the window-to-wall ratio to 0.3, and complete the building form settings. Next, create the Dragonfly model and name it Downtown, import it into DF Assign Model UWG Properties, and set the topography and the maximum sensible human heat flux to 20 W/m²

to complete the urban parameter settings. Finally, perform the microclimate simulation using the DF Run UWG operator, setting the vegetation albedo to 0.35, inputting the weather station parameters, urban boundary layer parameters and the original EPW file, and finally, starting the calculation and outputting the modified urban neighborhood weather file.

2.3.2. Wind Environment Simulation Module Setup

In order to further explore the relationship between the morphological layout of coastal city blocks and the wind environment, the wind simulation is based on the climate simulation using Grasshopper's plug-in Butterfly, which creates and runs computational fluid dynamics (CFD) simulations using OpenFOAM with the help of the open-source Python library. OpenFOAM is currently the most authoritative open-source CFD modeling engine used in research, and it is widely used in fluid dynamics computational research [44,45]. In addition, Butterfly can quickly export models created in Rhinoceros or Grasshopper to OpenFOAM and run several common airflow simulations related to building design, including simulating outdoor wind environments for urban spaces, simulating indoor airflows for thermal comfort and ventilation efficiency, and other related simulation tasks [46].

The neighborhood wind environment simulation involves six steps: processing model information, generating the geometry model, building the wind tunnel, subdividing the mesh, calculating the results, and visualizing the data. The numerical simulations in this paper will be performed using the RNG $k-\varepsilon$ turbulence model studied by Du et al. [47,48]. At the entrance, the average wind speed U , turbulence kinetic energy K and turbulence dissipation rate ε of atmospheric boundary layer (ABL) conditions refer to the simulation standard of P.J. Richards et al. [49]. The calculation principle and formula are as follows:

$$U_z = \frac{U_{ref}}{k} \ln \frac{z + z_0}{z_0} \quad (1)$$

$$j(z) = \frac{U_{ref}^2}{\sqrt{C_\mu}} \quad (2)$$

$$k(z) = \frac{U_{ref}^2}{\sqrt{C_\mu}} \quad (3)$$

where z_0 is the aerodynamic roughness length, which will be different for different terrain [50]. In this study, $z_0 = 1.0$ is taken to denote the dense building area. z is the height coordinate, U_{ref} is the reference wind speed at $z = 10$ m, $j = 0.42$ is the von Karman constant, and $C_\mu = 0.09$ is the turbulence model constant. The computation mainly revolves around the Butterfly Solution operator. After connecting the case output from Butterfly_SnappyHexMesh, the computation is carried out according to the relevant parameter settings, and finally, the vector data of the wind speed is output as the output solution and visualized.

2.3.3. Thermal Comfort Simulation Calculation Module Setup

In the simulation study, the methodology of the UTCI as a thermal environment assessment index for research is quite mature, so in this simulation of the thermal environment assessment process, the same UTCI is used as in the assessment of thermal environment indexes [36,51]. The calculation of the UTCI requires four parameters: wind speed, air temperature, average radiant temperature, and air humidity. The wind speed defaults to that at 10 m height or 1.5 times the wind speed at pedestrian height. In this study, the wind speed calculated by the wind environment simulation tool is used in the outdoor thermal comfort calculations to enhance accuracy. The thermal environment is calculated in three steps: first, T_{mrt} is calculated using the "Outdoor Solar MRT" operator in Ladybug, limited to the study period (winter solstice: 22 December, 6:00–18:00), with the ground reflectance

set to 0.25 and the average skin/clothing absorptance also set to 0.25. Subjects are assumed to face away from the Sun at a 45° angle and engage in walking.

2.3.4. Evaluation Factor Calculation Module

In addition to the thermal comfort and wind environment, the parameter evaluation factors for measuring the neighborhood layout include the neighborhood volume ratio, building density, and sky visibility factor. The volume ratio can be calculated by using the Gene Pool in Grasshopper to calculate the base area of each single building, multiplying the base area of each small unit by the corresponding number of floors of the unit to obtain the total area of each single building, and then using the Mass Addition Module to sum the total area of the nine single buildings, and then dividing it by the block area, so the optimized block can be calculated. The optimized block area is then divided by the block area to calculate the optimized block area. Similarly, the Mass Addition module is used to calculate the building density by adding and summing the base areas of the nine individual buildings and dividing by the block area.

The sky visualization factor needs to use the Populate 2D battery in Ladybug to scatter 20 test points randomly inside the block and at the same time access the center interface of the Sky Mask battery. Then, input the parameterized building information into the context port and set the number of sky patch splits to 3, as when the value is set to 3, the calculation accuracy is high and the error between the sky visualization and the real value is less than 1%. The size of the sky dome model is set to 0.2, and then the sky visibility factor corresponding to all the test points is obtained in the output port of sky_view. The calculation results of the points are added up and divided by the number of test points to obtain the average sky visibility factor of the neighborhood.

2.4. Multi-Objective Optimization Module Setup

The multi-objective optimization algorithm refers to the existence of multiple conflicting objectives, used to find a set of optimal solutions, so that each objective function can achieve the optimal state. In this paper, we mainly use the genetic algorithm in multi-objective optimization, which is similar to the simulation of the evolutionary process in nature and approaches the optimal solution through continuous iterative evolution, and this has been applied in several urban case studies [52–56]. The essence of optimization algorithms is genetic algorithms, and multi-objective optimization algorithms based on genetic algorithms have some basic characteristic parameters, which determine the algorithm's computational efficiency and have an important impact on the algorithm's performance [57,58]. In this study, Wallacei was chosen as a multi-objective optimization tool for the optimization study in the simulation. Wallacei has been proven to be reliable in several studies by using genetic algorithms to explore the relationship between the relevant design parameters set and the optimization metrics to arrive at the optimal block morphology design solution [58,59]. Table 3 briefly describes the optimization parameters and parameter settings in the Wallacei operator interface.

An optimization experiment was designed using the Grasshopper platform, with the controlled morphology factors as the design variables and the site-averaged wind speed and UTCI in winter and summer as the optimization targets. Due to the specific heat capacity of seawater, the coldest day of winter in the coastal area is one month later than the winter solstice in the inland area, and the cold wind in winter causes extreme discomfort, so the simulation time in winter is set to 22 January. Before the Grasshopper simulation, we need to input the boundary conditions, such as the simulation date (22 January), the beginning of the experiment at 8:00, the end of the experiment at 16:00 (including most of the pedestrians' outdoor activities), and the initial wind speed (with reference to the measured average wind speed of the site), etc. The simulation data are inputted as in Table 4.

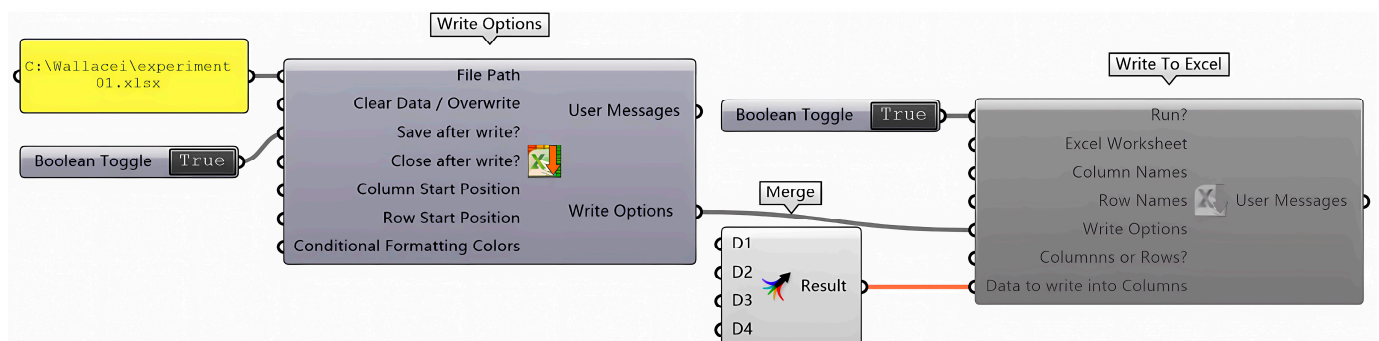
Since Wallacei is unable to record the data of the simulation process during the optimization process, it is necessary to use the TT Toolbox plug-in to satisfy this demand, so as to organize and analyze the data at a later stage (Figure 5).

Table 3. Wallacei optimization parameter setting instructions.

Optimization Parameters	Description of the Role	Parameterization
Crossover Probability	Measures the probability of two individuals crossing over, the larger the value, the faster the rate of emergence of a new type of population, generally takes the value 0.1–0.99.	0.9
Mutation Probability	The probability of mutation of the solution generated by the crossover affects the convergence process of the operation and the comprehensiveness of the solution.	-
Crossover Distribution Index	Smaller values imply that the crossover process retains more of the parent’s characteristics.	20
Mutation Distribution Index	A large value means that more variation is introduced in the crossover process. Smaller values mean that more of the parent’s characteristics are retained during the mutation process.	20
Random Seed	A large value means that more variation is introduced in the mutation process. The value determines how the algorithm is initialized.	1
Population Size	The number of populations involved in the evolution, usually 20–100.	20
Max Generations	The number of generations of evolution, with 0 meaning that the computation will continue until it is stopped manually.	50

Table 4. Analog parameter setting.

Experimental Season	Winter	Summer
Experimental dates	22 January	21 July
Simulation time	08:00–16:00	08:00–16:00
Initial wind speed (at 10 m)	3.3 m/s	3 m/s
Initial wind speed (at 1.5 m)	2.1 m/s	1.96 m/s
Fig. trends (esp. unpredictable ones)	N	SE

**Figure 5.** Data logging and export module for multi-objective optimization processes.

2.5. Optimized Simulation for Real Urban Neighborhood Case Simulation

2.5.1. Overview of Study Cases

Study case: the city of Dalian is located in the northeast of China, between 120 degrees 58 min and 123 degrees 31 min east longitude and 38 degrees 43 min and 40 degrees 10 min north latitude, and it is part of Liaoning Province. With a resident population of 7.539 million as of 2023, it is the window for foreign trade in northern China and a famous coastal tourist city. As a typical cold coastal city in China, Dalian’s climate is mainly influenced by three aspects: cold climate, “heat island effect” and ocean. In response to the climatic characteristics of the Dalian area, which is characterized by long and cold winters, a high wind speed and an unstable wind direction throughout the year, the selection of the practice neighborhoods is based on the Dalian LCZ climate zoning in the study by Zhao et al. [60]. Through the statistics of the LCZ maps, it is found that LCZ4 is mainly distributed in the coastal area, so the thesis will choose the neighborhoods in the open high-rise zone as the practice neighborhoods.

After determining the type of simulated neighborhood, this case selects Dalian Yixing Ocean Neighborhood as a case, which is located in Shahekou District, Dalian City, Liaoning Province (Figure 6). It was built in 2005, with a land area of 120,000 m², a building area of 380,000 m², a floor area ratio of 3.17, a green area ratio of 45%, and a parking space of 3405, with a total of 26 buildings, and it is a neighborhood that includes medium- and high-rise buildings. The neighborhood is surrounded by convenient traffic and a high flow of people, and it is close to many buses and Dalian Metro Line 1, with the coastline to the south, the marina to the west, and Xinghai Square to the east, making it a typical case of a coastal neighborhood.

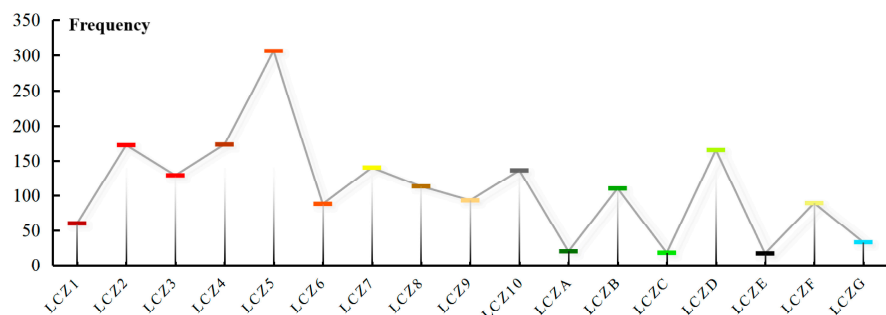
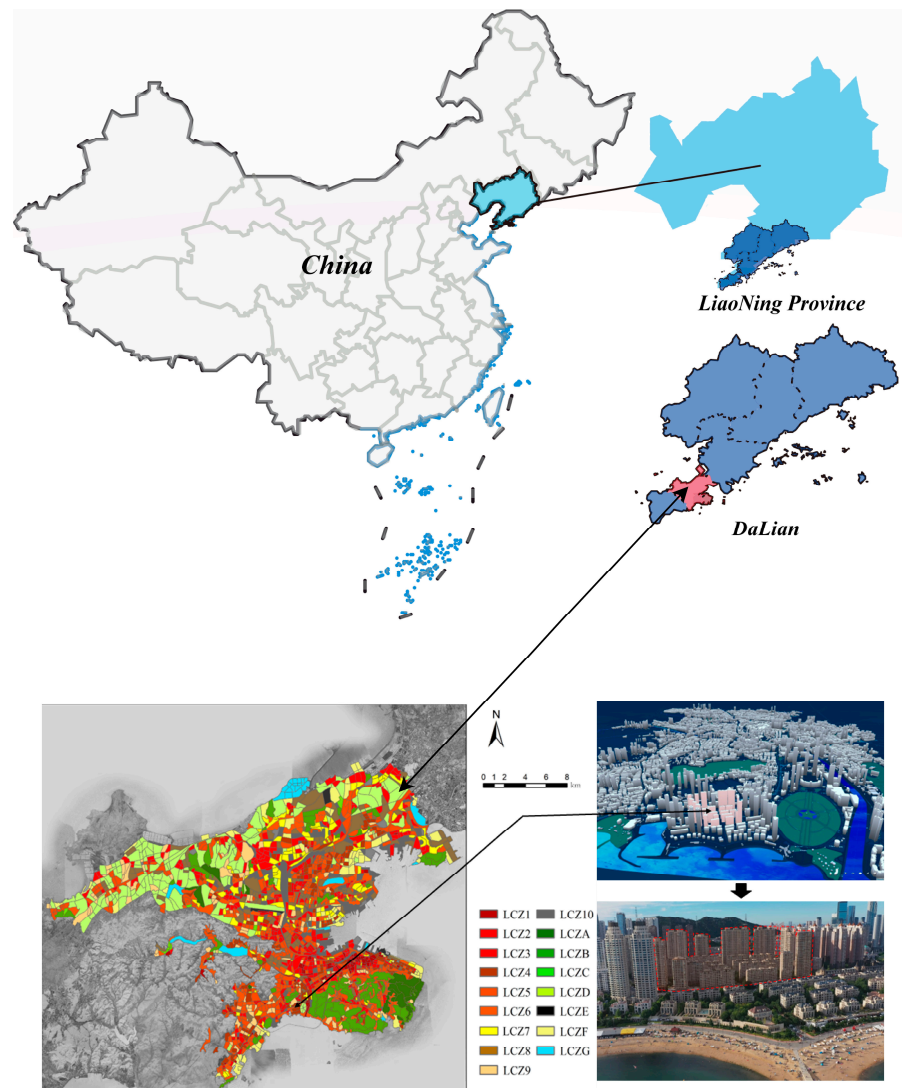


Figure 6. Map of Dalian City location and study area LCZ, and aerial photographs of the area.

2.5.2. Field Data Collection and Modeling

Dalian is too cold and windy in winter, and the sunset time in winter is around 16:00 p.m. Therefore, the research time of this study was chosen as the coldest day of winter (22 January 2024, 8:00–16:00) and the hottest day of summer (21 July 2023, 8:00–16:00) in Dalian. The points for collecting the wind speed were set at one each of the North Gate, South Gate, West Gate, East Gate, and Interior Center of One Star Ocean, for a total of five points. The measurement method involved placing the instrument for measuring the wind speed, i.e., portable weather station Kestrel 5500, at the collection points. The location of the collection points and the installation of the instrument are shown in Figure 7. To perform the measurements, the weather station Kestrel 5500 was set at a height of 1.5 m above the ground and was set to record wind speed at 1 min intervals, and its performance and use complied with ISO and national standards.



Figure 7. On-site measured points and instrument models.

Because the block model was too large for single building mapping, the block was parametrically modeled primarily using the Geographic Information System and the Elk plug-in.

The generated parametric model is numbered to facilitate the subsequent analysis of the building. From Figure 8, we can see that the block includes a total of 30 buildings, of which buildings No. 3, No. 7, No. 13, No. 25, and No. 28 are ground-floor stores with a height of 8.4 m; buildings No. 9–12, No. 14–17, No. 20–22, and No. 26–27 are mid-rise residential buildings with a height of 42 m; and the other buildings are high-rise, with a height of 93 m. The height of the other buildings is 93 m. After building the parameterized model of the actual case, it is necessary to conduct a preliminary assessment of the thermal comfort and wind environment of the case model, which is the same as the simulation assessment process in the ideal model.

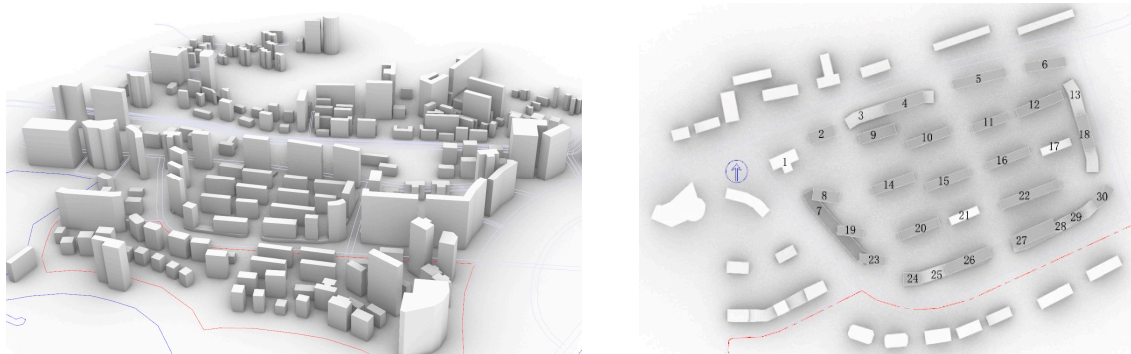


Figure 8. Parametric modeling and building numbering.

3. Analysis and Results

3.1. Ideal Model Control Group Simulation Results

3.1.1. Simulation Results for Control Groups with Different Neighborhood Types

Modeled according to the ideal model classification in Figure 3, 20 sets of experimental data were obtained after the simulation and computation, which were divided into four groups, A, B, C, and D, corresponding to different neighborhood types. A control group was set up for each group according to the neighborhood morphology control factor (Table 2). The simulated and calculated wind environment and UTCI results for the four neighborhood types were ranked according to the magnitude of the values (Figure 9). As can be seen from the figure, in the distribution of the mean value of the wind speed for the block types, panel high-rise building > point building > panel mid-rise building > enclosed building; in the distribution of the mean value of the UTCI for the block types, enclosed building > panel mid-rise building > panel high-rise building > point building.

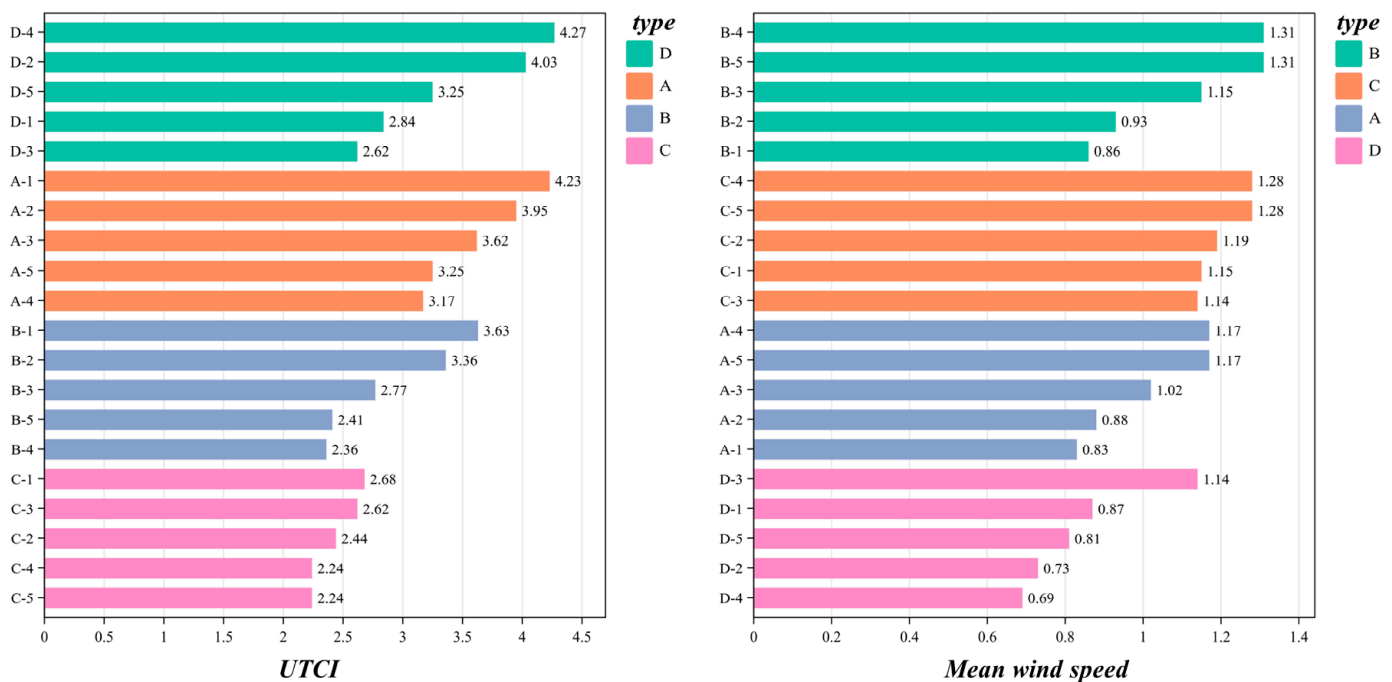


Figure 9. Results of the UTCI vs. the average wind speed simulations for different neighborhood types.

Figure 10 shows the boxplots of the mean wind speed and UTCI distribution for each neighborhood type on the coldest day of winter. The results indicate that type B neighborhoods have the widest average wind speed range, from 0.86 to 1.31 m/s, with a difference of 0.15 m/s. In contrast, type C neighborhoods have the narrowest average wind speed range, from 1.14 to 1.28 m/s, with a difference of only 0.14 m/s. Type D neighborhoods show a significantly higher range of UTCI values, distributed between 2.62 and 4.27 °C, reflecting differences due to various enclosure methods and heights. Meanwhile, type C neighborhoods exhibit the narrowest UTCI distribution, ranging from 2.24 to 2.68 °C, indicating a high degree of stability.

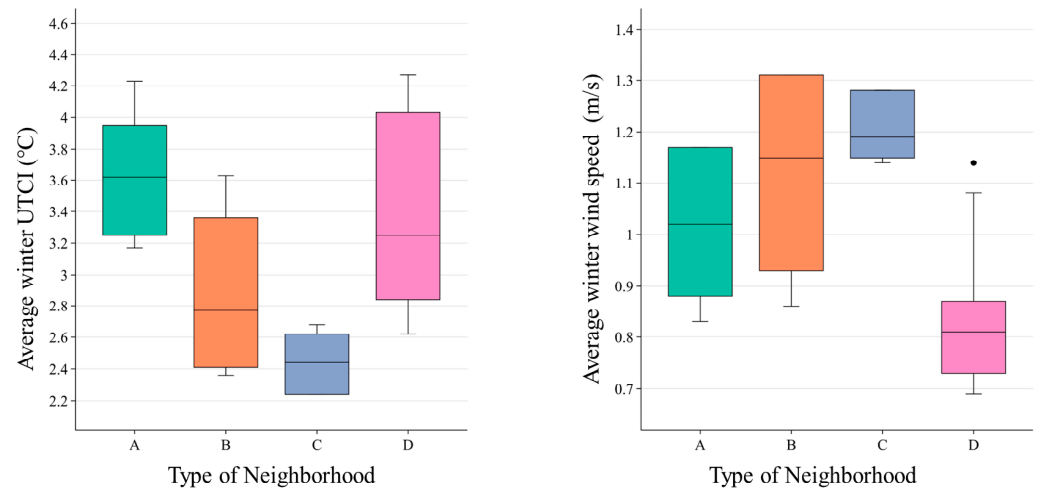


Figure 10. Boxplots of the distribution of the mean site wind speed and UTCI for each neighborhood type.

3.1.2. Building Orientation Control Group Simulation Results

To accurately compare the control variables, this simulation only changed the building orientation while analyzing all the control groups, and the results are shown in Figure 11. The comparison shows that the changes in the building orientation for neighborhood types A and B are consistent with the changes in the mean values of the wind speed and UTCI. When the building orientation is due south or north, the mean wind speed is the lowest (A-1 is 0.83 m/s, B-1 is 0.86 m/s). As the orientation increases, the wind speed gradually rises, reaching its maximum at 45 degrees (A-1 is 1.17 m/s, B-1 is 1.31 m/s). The mean UTCI is the highest when the orientation is due south or north (A-1 is 4.23 °C, B-1 is 3.63 °C), and lowest at 45 degrees (A-1 is 3.17 °C, B-1 is 2.36 °C). Additionally, for building orientations of 45° northeast and 45° southeast, the wind speeds are the same, but the UTCI is slightly higher for the southeast orientation.

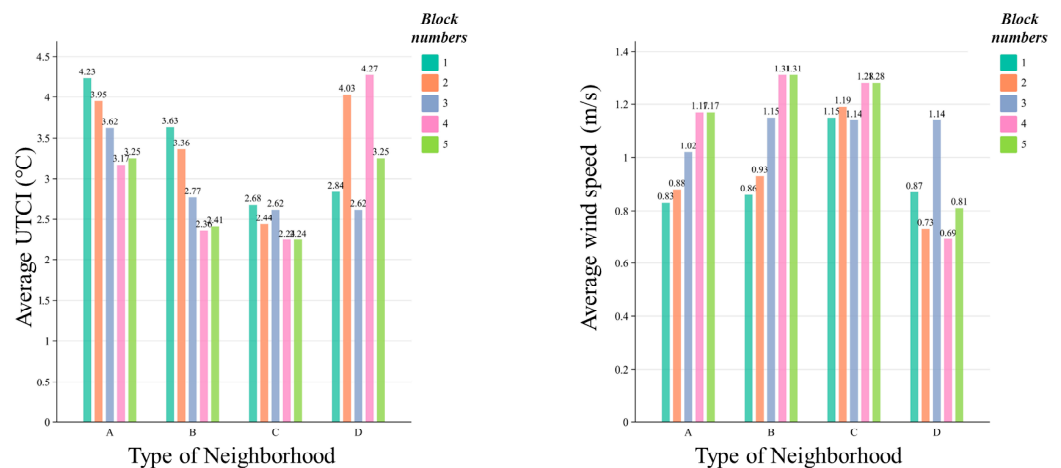


Figure 11. Calculated wind speed and UTCI in the control group with different building orientations.

3.1.3. Simulation Results for the Control Group of Building Floors

To explore the relationship between the building height, wind speed, and UTCI mean values, the simulation only varied the building height, establishing five control groups: mid-rise slab buildings (Group A) and high-rise slab buildings (Group B). Figure 12 shows the comparison of the wind speed and UTCI mean values for both types. The results indicate that the average wind speed of the mid-rise buildings is slightly lower than that of the high-rise buildings, with the smallest difference in Group 1 at 0.03 m/s and the largest in Groups 4 and 5 at 0.14 m/s. Additionally, the UTCI mean value for the mid-rise

buildings is noticeably higher than for the high-rise buildings, with the smallest difference in Group 2 at 0.59 °C and the largest in Group 3 at 0.85 °C.

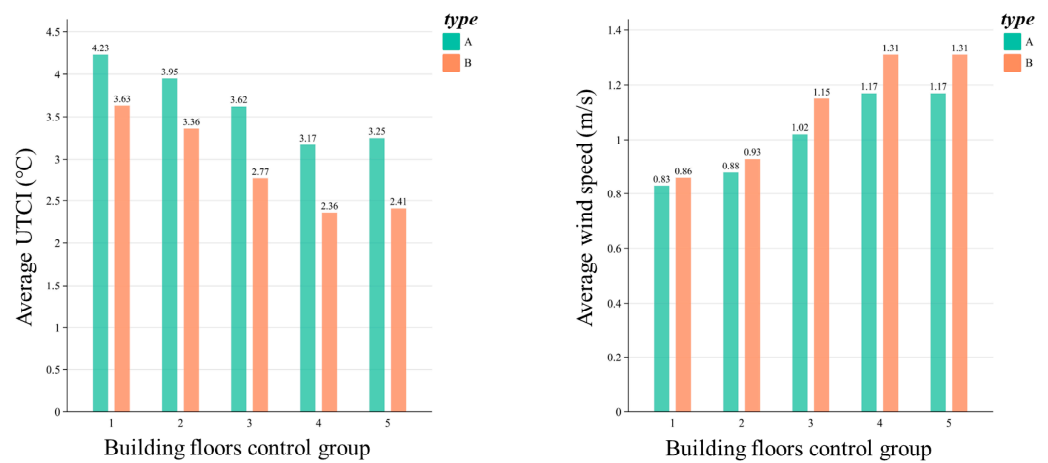


Figure 12. Calculation of the wind speed and UTCI in the control group of different building floors.

3.2. Analysis of Results Based on Multi-Objective Optimization

3.2.1. Preliminary Analysis of Optimization Results

This multi-objective optimization experiment is based on the Grasshopper design platform, utilizing the Wallacei (V 2.7) tool to select the building density, floor area ratio, and SVF as independent variables, and the average wind speed and UTCI in winter and summer as optimization objectives, employing an evolutionary algorithm for the optimization. Each generation optimizes 20 genes over a total of 50 iterations, amounting to 1000 genes, with a total time of about 398 h and an average computational time of 23.88 min per case (Figure 13). The Wallacei platform automatically stops when the set number of iterations is reached, so it is necessary to assess whether the optimization has converged after the specified iterations to ensure the accuracy of the generated non-dominated solution set.

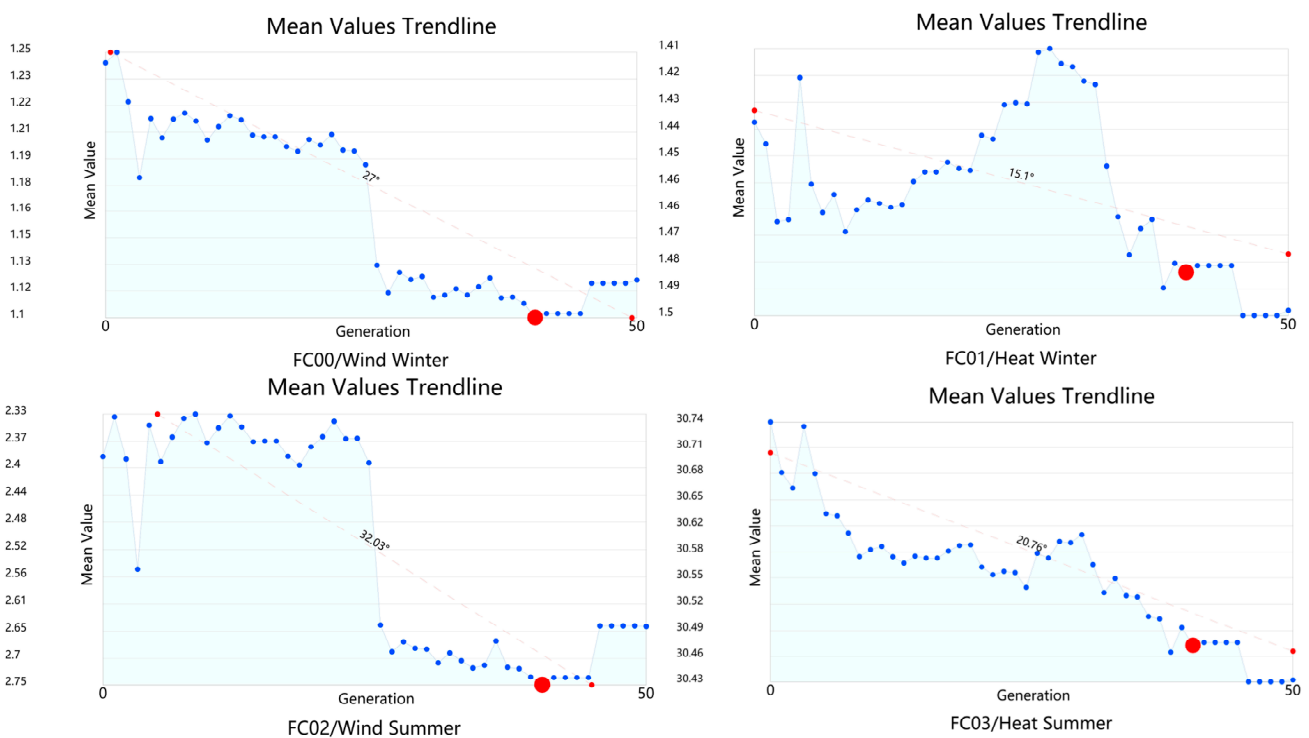


Figure 13. Mean trendline for 50 iterations of 4 optimization objectives.

The Wallacei tool visualizes the trend of the optimization objective through a 3D coordinate system, where each point represents an optimized solution. The x, y, and z axes correspond to the winter wind speed, winter UTCI, and summer wind speed, respectively, and the color of the point indicates the summer UTCI, with a darker green color indicating a better optimization (Figure 14). The closer the point to the origin, the better the overall performance. The big blue ball represents the comprehensive optimal solution, which is not the optimal one for each index but the average optimal one.

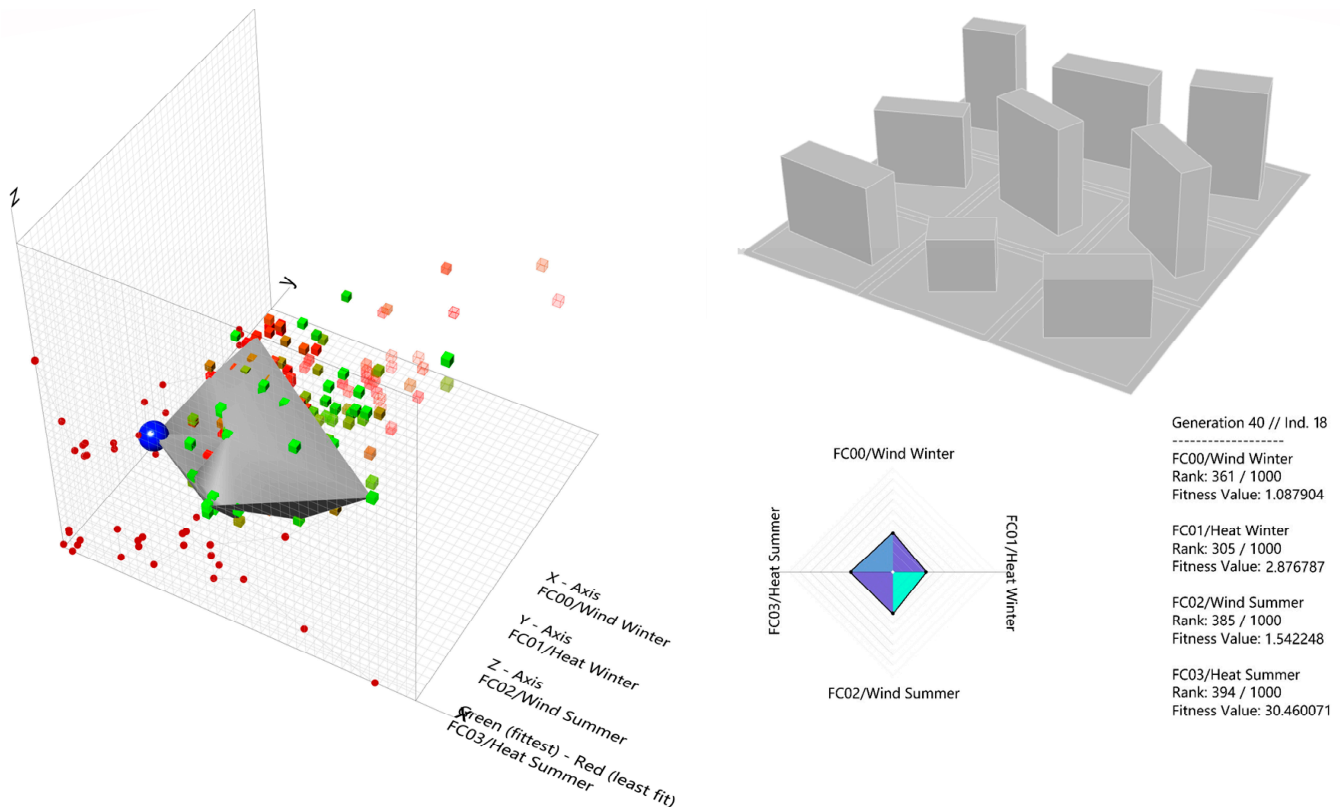


Figure 14. Multi-objective optimization solution set distribution and average optimal solution shape.

The light gray area in the 3D coordinates represents the Pareto front surface, which includes all the non-dominated solutions and reflects the mutual constraints among the performance objectives. In multi-objective optimization, the solutions are categorized into non-dominated solutions (optimal solutions) and dominated solutions. Non-dominated solutions optimize one performance without significantly sacrificing others, while dominated solutions indicate that there is room for further optimization. Analyzing the set of non-dominated solutions allows for an in-depth exploration of the optimization effects, especially among solutions with similar levels of integrated microclimate performance.

3.2.2. Non-Dominated Solution Set Analysis (DSSA)

Figure 15 shows the neighborhood morphology map and cluster analysis of the 28 non-dominated solutions from the Pareto front surface. To analyze these solutions, representative neighborhood morphologies were extracted through clustering. The x, y, and z axes represent the mean winter wind speed, mean winter UTCI, and mean summer wind speed, respectively, while the mean summer UTCI is implied. The five colors (red, blue, green, yellow, and purple) indicate five clusters, with the points in each cluster representing similar scenarios and the cluster center showing the average location of all the points.

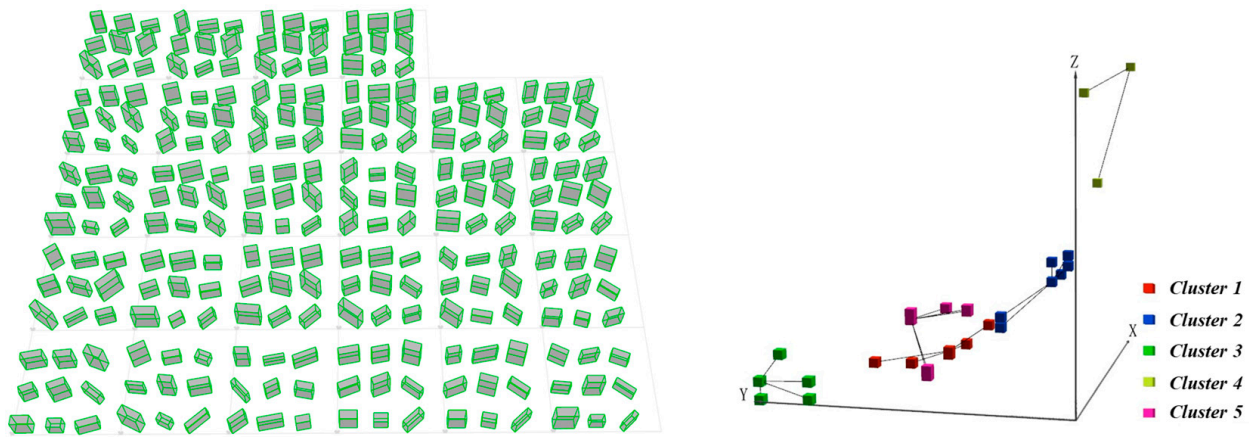


Figure 15. Multi-objective optimization solution set distribution and cluster analysis.

Table 5 shows the results of the clustering and sub-clustering, which combined with the location of the distribution of non-dominated solutions on the x, y, and z axes in Figure 15, shows that Cluster 3 and Cluster 4 are located at the end of the overall non-dominated solutions. As a result, Cluster 3 has the lowest mean winter wind speed and summer wind speed, but the highest mean winter UTCI. Cluster 4, on the contrary, has the highest mean winter wind speed and summer wind speed and the lowest mean winter UTCI. In contrast, the performance of Clusters 1, 2 and 5 is more balanced.

Table 5. Non-dominated solution clustering results.

Clustering Category	Number of Clusters	Center of Clustering			
		Winter Wind Speed Average (m/s)	Winter UTCI Mean Value (°C)	Summer Wind Speed Average (m/s)	Summer UTCI Mean Value (°C)
Cluster 1	6	1.06	3.07	1.48	30.85
Cluster 2	7	1.17	2.60	1.60	30.28
Cluster 3	5	0.98	3.31	1.30	30.83
Cluster 4	3	1.47	1.70	1.67	30.31
Cluster 5	7	1.05	2.81	1.44	30.23

Figure 16 shows the non-dominated solution block patterns of the five clusters, with the block pattern at each cluster's center considered the optimal layout. Cluster 3 features two rows of lower buildings in the south and center, with higher buildings in the north, which helps to capture sunlight and block northern winds in winter, resulting in the best winter wind–heat comfort. In contrast, Cluster 4 has taller buildings that increase the shaded areas, but the lower height of Building 6 allows more southeasterly winds in summer, making it the best for summer wind–heat comfort.

Cluster 5 integrates the layout characteristics of Clusters 3 and 4. The southern buildings have lower heights, allowing more sunlight into the block; the middle building is taller, providing shade for the northern part; and the northern buildings are relatively high, blocking winter winds from the north. Building 6, across all the scenarios, has a lower height and faces southwest, facilitating the entry of southeasterly winds in summer. Building 0, on the other hand, is taller, with a larger facade, effectively blocking summer sunlight and maximizing economic benefits. Overall, the layout with high buildings on the northwest and lower buildings on the southeast allows southeasterly winds to cool the site in summer while effectively blocking northern winds in winter.

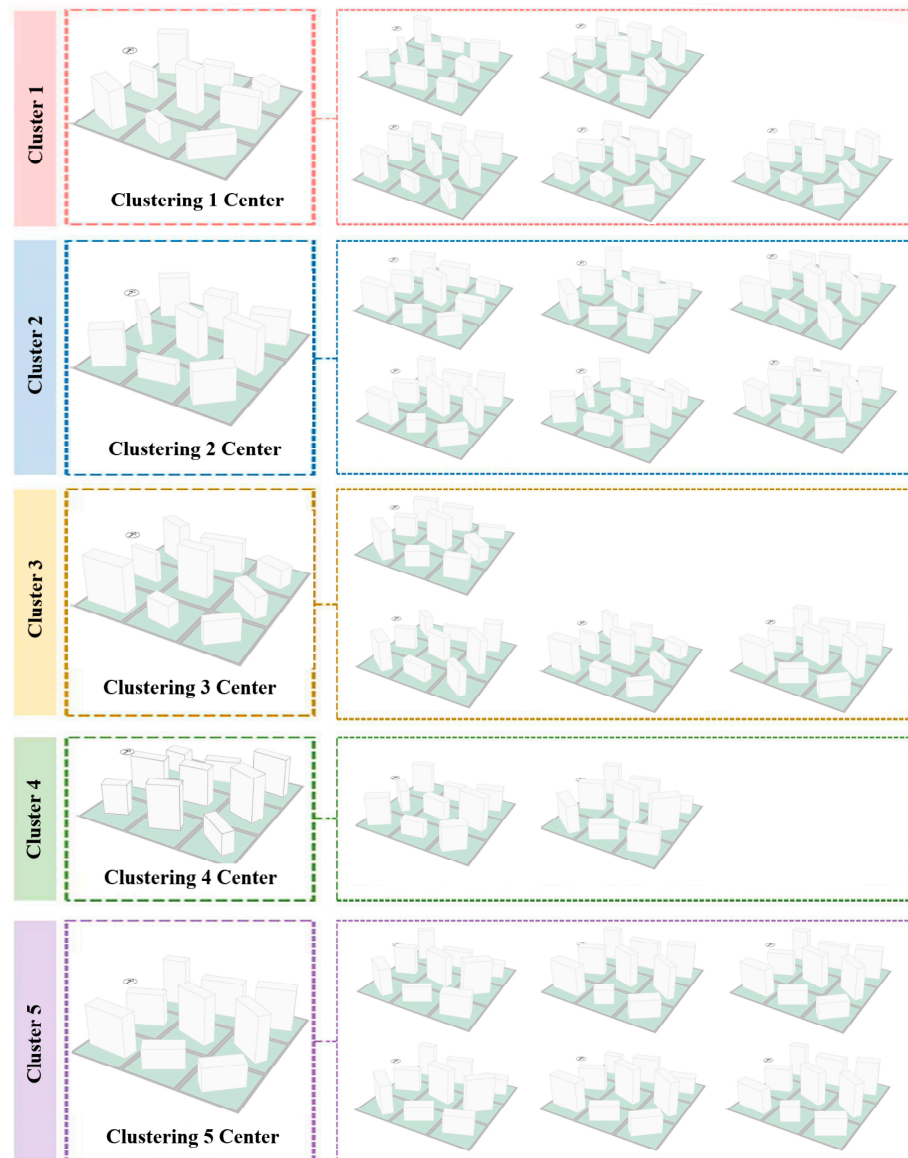
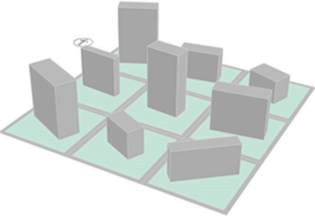
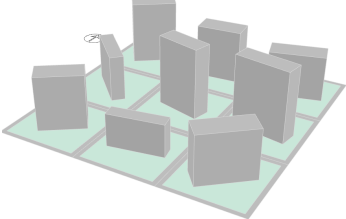
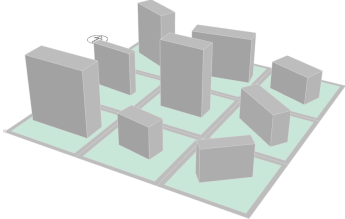
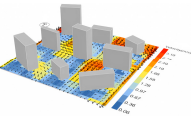
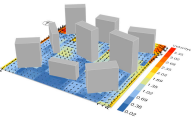
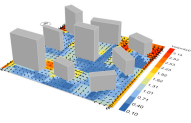
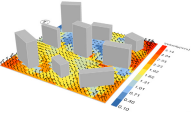
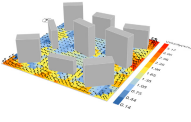
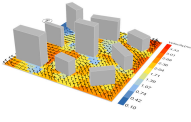
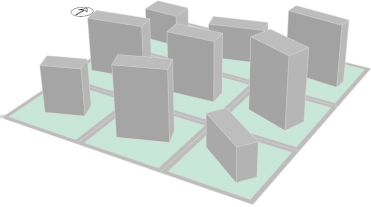
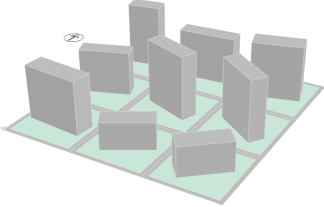
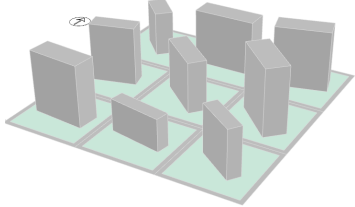
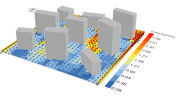
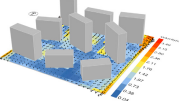
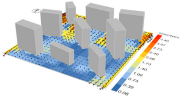
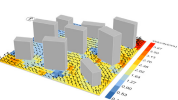
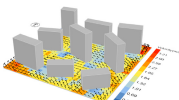
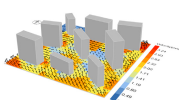


Figure 16. Neighborhood morphology of the non-dominated solution sets for the 5 clusters.

In order to show more clearly the differences between the optimization objectives of the different clustering morphology goals, five clustering centers and one feasible solution are selected as representative schemes in Table 6, respectively. The four small schematic diagrams below the axonometric schematic of each solution, representing the mean winter wind speed, mean winter UTCI, mean summer wind speed, and mean summer UTCI, from left to right and top to bottom, can visualize the focused optimization points of each clustered representative solution.

The performance of the clusters in the table indicates that to enhance the thermal comfort in the neighborhood during winter, the height of the buildings on the south side should be reduced, while the height of the buildings in the middle and north should be increased to boost the economic benefits, considering sunlight from various angles. Overall, the building height layout can be summarized as “high in the north and low in the south” and “high in the northwest and low in the southeast”, which is more conducive to the target performance. This layout allows most of the block to be well lit, guides the summer southeasterly wind into the block to remove excess heat, and the taller buildings on the west can reduce the impact of western sunlight while providing shade for the interior. Additionally, the high-rise buildings on the northwest can block the winter north winds, improving the winter wind–heat comfort.

Table 6. Each clustering parameter and analysis.

Cluster Center 1: Gen2 Ind09		Cluster Center 2: Gen38 Ind18		Cluster Center 3: Gen33 Ind01	
					
					
					
FAR: 2.13	BD: 12.14%	FAR: 2.87	BD: 14.40%	FAR: 2.36	BD: 13.24%
FC00: 1.06 m/s	FC01: 3.07 °C	FC00: 1.17 m/s	FC01: 2.60 °C	FC00: 0.98 m/s	FC01: 3.31 °C
FC02: 1.48 m/s	FC03: 30.85 °C	FC02: 1.60 m/s	FC03: 30.28 °C	FC02: 1.30 m/s	FC03: 30.83 °C
Cluster Center 4: Gen0 Ind19		Cluster Center 5: Gen34 Ind16		Optimal solution: Gen25 Ind10	
					
					
					
FAR: 2.24	BD: 10.84%	FAR: 3.28	BD: 16.53%	FAR: 3.10	BD: 14.95%
FC00: 1.47 m/s	FC01: 1.70 °C	FC00: 1.05 m/s	FC01: 2.81 °C	FC00: 1.15 m/s	FC01: 2.61 °C
FC02: 1.67 m/s	FC03: 30.31 °C	FC02: 1.44 m/s	FC03: 30.23 °C	FC02: 1.41 m/s	FC03: 30.42 °C

However, design decisions need to weigh multiple factors, although the multi-objective optimization algorithm has screened out balanced and excellent solutions and eliminated many poor solutions. However, due to the mutual constraints between the indicators, it is still difficult to find a comprehensive and perfect program. Therefore, when selecting the program, it should be selected according to the focus. Based on the above analysis, the performance characteristics of the five clusters on the four optimization flags are summarized, and the number of ☺ is used to indicate the strength of the performance, as shown in Table 7.

Table 7. Evaluation of the characteristics of each cluster.

Clustering Category	Winter Wind Speed Average (m/s)	Winter UTCI Mean Value (°C)	Summer Wind Speed Average (m/s)	Summer UTCI Mean Value (°C)
Cluster Center 1	☺☺☺	☺☺☺☺	☺☺	☺☺
Cluster Center 2	☺☺	☺☺	☺☺☺☺	☺☺☺
Cluster Center 3	☺☺☺☺☺	☺☺☺☺☺	☺	☺
Cluster Center 4	☺	☺	☺☺☺☺☺	☺☺☺☺☺
Cluster Center 5	☺☺☺☺	☺☺☺	☺☺☺	☺☺☺☺

3.3. Comparative Analysis Results before and after Optimization of Real Urban Community Cases

3.3.1. Status of the Neighborhood Wind–Heat Environment before Design Optimization

Before optimizing the real neighborhood case, it is necessary to simulate and evaluate the wind environment and thermal comfort of the existing real neighborhood in winter and summer (the coldest day and the hottest day) in order to analyze the problems and deficiencies of the current wind and thermal environment of the neighborhood and to propose targeted strategies to address these deficiencies. Figure 17 shows the visualization results of the wind and thermal environments in winter and summer for the parametric model based on the real neighborhood before optimization.

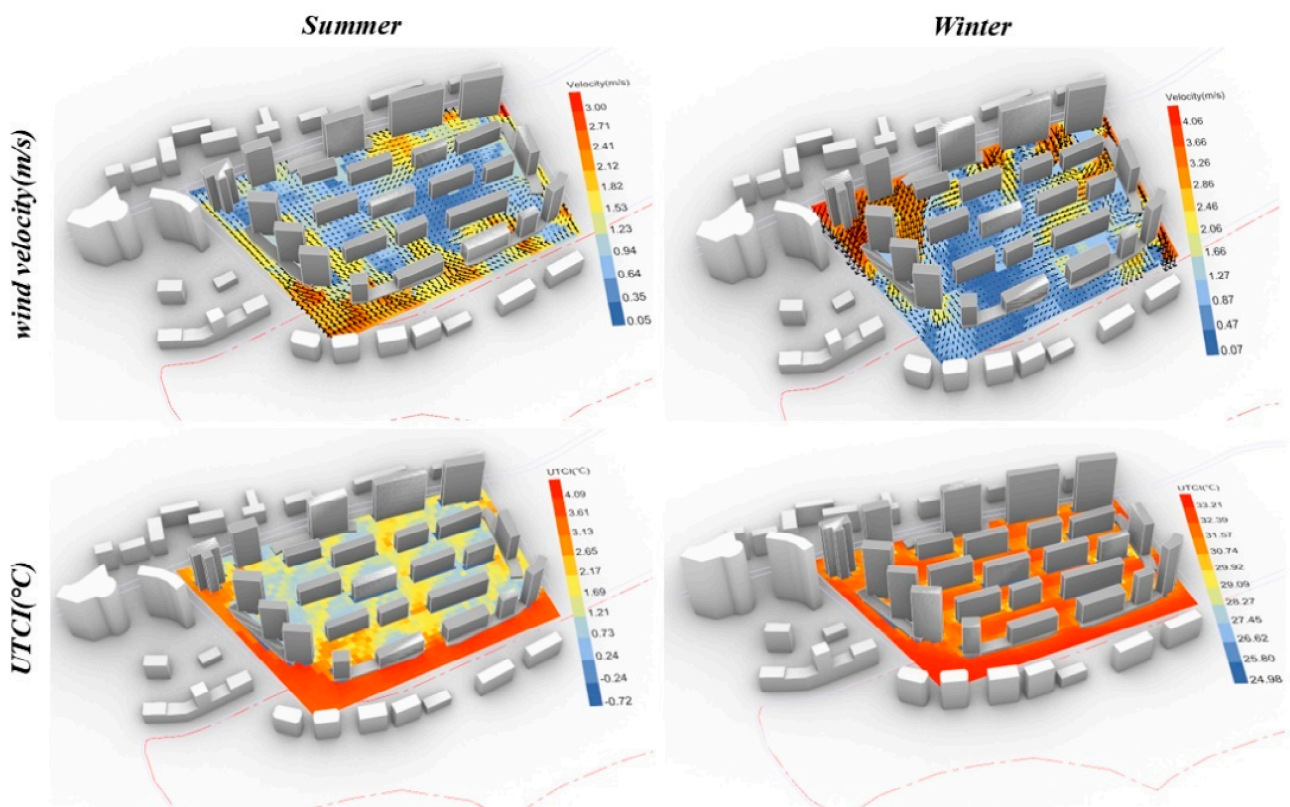


Figure 17. Calculated results of the wind–heat environmental assessment for the winter and summer seasons (before optimization).

Figure 17 shows that on the coldest winter day, the neighborhood’s wind environment is poor, with a maximum wind speed of 4.06 m/s, an average of 1.5 m/s, and a comfort zone ratio of 42%. Although the surrounding buildings use a semi-enclosed layout to reduce the wind speed, the height and density of the northern buildings create a tunnel effect, leading to significantly higher wind speeds and discomfort for residents.

On the hottest summer day, the wind environment performs even worse, with a maximum wind speed of only 3.00 m/s, an average of 1.08 m/s, and a comfort zone ratio of 39%. The center of the neighborhood has large areas of no wind and low wind zones, with speeds dropping below 1.0 m/s, and in some areas even below 0.35 m/s. According to the pedestrian wind environment zoning table, these areas are classified as low wind speed zones, where pedestrians can hardly feel airflow in the hot summer, resulting in poor thermal comfort [61]. There are many southeast winds along the Marina in summer, but due to the podiums set up in the southeast direction of the block, the overall central area has a small opening on the windward side, which blocks the inflow of summer winds, resulting in a larger area of low wind.

The UTCI distribution shows that on the coldest winter day, the thermal environment is poor, with a highest UTCI of 4.09 °C, a lowest of −0.72 °C, and an average of 1.24 °C. The high surrounding buildings create shade, reducing the solar radiation and lowering the UTCI values. On the hottest summer day, the UTCI ranges from 33.21 °C to 24.98 °C, averaging 30.42 °C, primarily in the unshaded south and west, but the overall performance remains poor.

3.3.2. Neighborhood Optimization Strategy and Post-Optimization Results

To address the wind and heat environment issues from the simulation, the block building form and site space design can be optimized. Based on the strategies extracted from the multi-objective optimization strategy, the following morphology design planning and height optimization strategies are used for the field blocks:

- i. Add a new low-rise podium or more greenery at the base of building No. 1 to block the north wind from the northwest area.
- ii. Partially demolish the podiums of buildings No. 13 and No. 29 to allow more southeasterly winds into the central area and improve the thermal comfort.
- iii. The heights of the middle buildings on the southeast and west sides will be reduced to meet sunlight needs (removing the top 5 floors of building No. 19 and the top 10 floors of building No. 30).

The buildings on the north side will remain unchanged to prevent winter cold winds. A specific schematic of the modifications is shown in Figure 18.

After optimizing the real neighborhood, the effectiveness of the wind–heat environment improvements needs to be evaluated. Figure 18 shows the visualized distribution of the optimized wind–heat environment. The simulation results indicate a significant improvement on the coldest winter day: the maximum wind speed decreased to 3.27 m/s, the average wind speed was 1.03 m/s, and the percentage of the comfort zone increased to 58%. After the retrofit, the maximum wind speed dropped by 0.79 m/s, the average by 0.47 m/s, and the comfort zone proportion rose by 16%. The new low-rise podium at the base of buildings 1–2 effectively blocked winds from the north, significantly reducing the strong wind zone in the northwest. In terms of thermal comfort, the conditions on the coldest day also improved, with a maximum UTCI of 2.78 °C, a minimum of 0.89 °C, and an average of 1.72 °C. Although the maximum UTCI decreased by 1.31 °C, the minimum UTCI improved by 1.61 °C, and the mean UTCI increased by 0.48 °C.

The wind environment and thermal comfort performance on the hottest day of the summer also improved. The maximum wind speed inside the neighborhood increased to 4.31 m/s, the average wind speed improved to 1.63 m/s, the percentage of wind environment comfort zone increased to 67%, and the wind-free zone decreased significantly. In terms of the thermal comfort performance, the maximum UTCI on the hottest day in summer decreased to 32.55 °C, the minimum value decreased to 24.37 °C, and the average UTCI was 29.83 °C, which was 0.59 °C lower than the average UTCI before the retrofit, and the overall thermal comfort in summer was significantly improved.

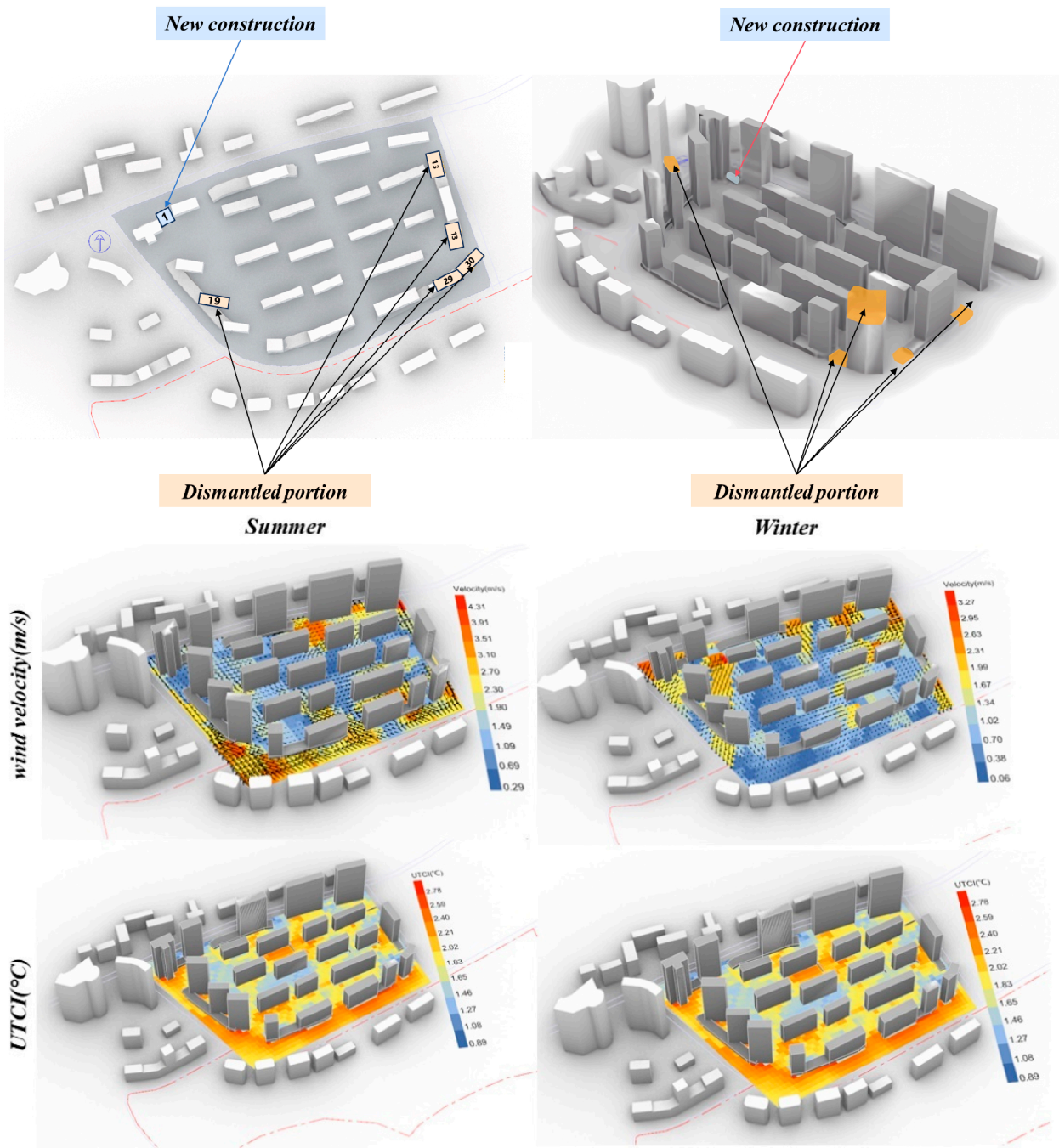


Figure 18. Schematic diagram of the optimized design measures and local thermal comfort after the retrofit.

4. Discussion

4.1. Ideal Model Optimization Strategy

The simulation process presented in this paper complements the shortcomings of previous related simulation studies as comprehensively as possible. For example, it complements the need for further analysis using Butterfly, as mentioned by Lenka Kabošová et al., in urban form optimization [62]. In addition, since the city is an extremely complex operating system, the morphology of the urban neighborhoods is also much more than the several simple combinations mentioned in this paper. In this paper, only the more representative forms of building enclosure in Dalian are selected for simulation and evaluation, but other

types of irregular forms in the city also occupy a certain proportion, which needs to be completed in the subsequent optimization of further classification and evaluation.

In the multi-objective optimization process of the ideal model in this study, among the four optimization objectives, except for the positive correlation between the average value of the summer wind speed and the average value of the UTCI, the other ones are in competition with each other. Therefore, the study of the microclimate in small neighborhoods should take into account the characteristics of the geographic conditions of the study area, and the case city Dalian is located in the cold coastal area, which needs to focus on insulation and wind shielding in winter compared to ventilation and heat dissipation in summer. When the needs of the winter and summer seasons cannot be satisfied at the same time, the winter microclimate comfort needs should be considered first. That is, mainly by adjusting the height of the buildings, adopting the layout of “high in the north and low in the south” and “high in the northwest and low in the southeast” to withstand the cold wind attack in winter, so as to improve the thermal comfort in winter and improve the overall microclimate.

4.2. Implementation Measures of Real Case Optimization

There are many cases of the optimization of real neighborhoods based on simulation evaluation, such as the simulation evaluation of the daylight and thermal performance of high-rise residential layouts by Wang et al. through a multi-objective optimization algorithm [63], and Zhang et al. generated residential layouts and optimized their performance through a multi-objective optimization algorithm [64], etc. However, through the concept of a non-dominated solution set, it can be concluded that the focus of urban design based on different objectives and performance optimization is completely different [65], and the multi-objective optimization needs to be combined with the local norms and climatic characteristics of the study area for targeted optimization, rather than blindly carrying out comprehensive optimization.

This study is not just a subjective proposal for transformation measures for a certain case but also an analysis of the optimization strategies based on the ideal model of the city as a whole. This method of rapid parametric modeling and analysis and determining the design threshold range is highly applicable in the early stage of urban design, especially because all the operations are based on the parametric platform Grasshopper, which solves the problems encountered in the process of urban design through a combination of various plug-ins. Without additional learning costs, designers can make informed decisions based on the numerical values of the problems and optimization suggestions at the early stage of the design process.

4.3. Research Deficiency and Limitation

In this study, the ocean wind is an important parameter for the urban wind and thermal environment, and if its influence on the overall wind and thermal environment of the city is further explored, the simulation study can be closer to the reality. However, this process requires long-term meteorological data or simulation data, so this paper does not explore the long-term impact of the ocean wind on the city. In addition to the wind conditions, the humid environment of coastal cities, particularly the air humidity, is also a significant factor influencing the wind–heat environment. However, due to space limitations, this article focuses primarily on the wind, which has a more pronounced impact on the thermal environment in winter.

Due to the limitations of the simulation conditions, this study only selected representative neighborhoods for the simulation evaluation and optimization to validate the effectiveness of the optimization method. The strategies and recommendations based on the ideal model remain quite limited. However, with the continuous development of artificial intelligence technologies, an increasing number of algorithm plug-ins will be integrated into the Grasshopper platform, expanding the scope of research and simulation in the future. By constructing a foundational environment and connecting to cloud servers,

it will be possible to simulate regional urban forms and wind–heat environments, resulting in more accurate and reliable urban design strategies.

5. Conclusions

In this paper, a comprehensive parametric wind–heat environment assessment method is proposed through the Rhino and Grasshopper platforms and based on previous research, and a complete set of initial urban design assessment processes is established by combining various plug-ins and applying multi-objective optimization algorithms to the initial urban design assessment. After a series of simulation optimization processes and analysis of the simulation results, the following conclusions are drawn.

1. The interrelationships between the wind and thermal environments of urban forms in different seasons are explored by establishing an ideal model, and a multi-objective optimization algorithm is used to provide a non-dominated solution set for the initial urban design. Five cluster centers are derived using cluster analysis, and the optimal feasible solution is generated after comparing the optimization performance of the five cluster combinations. The optimized wind environment and thermal comfort are significantly improved.

2. By analyzing the characteristics of the optimal feasible solution combination, it is concluded that, under ideal conditions, the block layout of Dalian City should follow the building layout of high northwest and low southeast, which can ensure that the southeast wind enters the interior of the site to take away the heat in summer, enhance the thermal comfort of the site's summer wind, and also effectively block the intrusion of the north wind on the interior of the block in winter.

3. Based on the optimization strategy derived from the ideal model for real neighborhoods in Dalian, it is found that the optimized average wind speed inside the neighborhoods in winter is reduced by 0.47 m/s and the UTCI is increased by 0.48 °C; in summer, the wind speed inside the neighborhoods is increased to 1.5 m/s and the UTCI is reduced by 0.59 °C.

In summary, the wind and heat environment in the winter and summer seasons can be effectively improved by optimizing the layout of the urban form, which provides a scientific basis for urban renewal design. These conclusions verify the practicality and effectiveness of the multi-objective optimization strategy in urban microclimate improvement, and they provide an important reference for future urban planning and design. Of course, this study has some limitations, including the presence of a large computational volume and urban locality factors, but with the continuous development of artificial intelligence and cross-disciplinary research, and as designers and programmers continue to develop interesting new features, Rhino's Grasshopper and related extensions and plug-ins are still evolving, meaning this workflow still has great potential.

Author Contributions: Conceptualization, S.X. and F.G.; methodology, D.Y. and S.M.; project administration, X.F.; resources, J.D.; validation, H.Z.; writing—original draft, S.X.; writing—review and editing, P.Z. All authors have read and agreed to the published version of the manuscript.

Funding: This research received no external funding.

Institutional Review Board Statement: Not applicable.

Informed Consent Statement: Not applicable.

Data Availability Statement: Data are contained within the article.

Conflicts of Interest: Author Xianchao Fan was employed by the company China Construction Industrial & Energy Engineering Group Co., Ltd. The remaining authors declare that the research was conducted in the absence of any commercial or financial relationships that could be construed as a potential conflict of interest.

Glossary

Name	Definition
MOO (multi-objective optimization)	Algorithms for handling objective optimization problems and finding optimal solutions.
UTCI (Universal Thermal Climate Index)	Indicator used to evaluate thermal comfort.
NDVI (normalized difference vegetation index)	A normalization index that describes the spatial distribution of vegetation, and the range is -1 to 1 .
FAR (floor area ratio)	An urban form factor that represents the ratio of overall floorage to research unit.
SVF (sky view factor)	The ratio at a point in space between the visible sky and a hemisphere centered over the analyzed location.
Az (azimuth)	Used to indicate the building orientation.
AVG (average wind velocity)	For assessment of the wind environment.
BD (building density)	The floor area of the building divided by the total area of the site.
BF (number of floors)	Used to indicate the number of floors in a building.
LCZ (local climate zone)	Classification methods used for urban localized thermal climates.

References

- Middel, A.; Häb, K.; Brazel, A.J.; Martin, C.A.; Guhathakurta, S. Impact of urban form and design on mid-afternoon microclimate in Phoenix Local Climate Zones. *Landsc. Urban Plan.* **2014**, *122*, 16–28. [\[CrossRef\]](#)
- Jagarajan, R.; Asmoni, M.N.A.M.; Mohammed, A.H.; Jaafar, M.N.; Mei, J.L.Y.; Baba, M. Green retrofitting—A review of current status, implementations and challenges. *Renew. Sustain. Energy Rev.* **2017**, *67*, 1360–1368. [\[CrossRef\]](#)
- Yuan, X.; Liu, X.; Zuo, J. The development of new energy vehicles for a sustainable future: A review. *Renew. Sustain. Energy Rev.* **2015**, *42*, 298–305. [\[CrossRef\]](#)
- Ren, G.; Ma, G.; Cong, N. Review of electrical energy storage system for vehicular applications. *Renew. Sustain. Energy Rev.* **2015**, *41*, 225–236. [\[CrossRef\]](#)
- Olunmi, O.A.; Xia, P.B.; Skitmore, M. Green building incentives: A review. *Renew. Sustain. Energy Rev.* **2016**, *59*, 1611–1621. [\[CrossRef\]](#)
- Zuo, J.; Zhao, Z. Green building research—current status and future agenda: A review. *Renew. Sustain. Energy Rev.* **2014**, *30*, 271–281. [\[CrossRef\]](#)
- Zhang, C.; Cui, C.; Zhang, Y.; Yuan, J.; Luo, Y.; Gang, W. A review of renewable energy assessment methods in green building and green neighborhood rating systems. *Energy Build.* **2019**, *195*, 68–81. [\[CrossRef\]](#)
- Crane, M.; Lloyd, S.; Haines, A.; Ding, D.; Hutchinson, E.; Belesova, K.; Davies, M.; Osrin, D.; Zimmermann, N.; Capon, A.; et al. Transforming cities for sustainability: A health perspective. *Environ. Int.* **2021**, *147*, 106366. [\[CrossRef\]](#)
- Nik, V.M.; Perera, A.; Chen, D. Towards climate resilient urban energy systems: A review. *Natl. Sci. Rev.* **2021**, *8*, nwa134. [\[CrossRef\]](#)
- Laino, E.; Iglesias, G. Extreme climate change hazards and impacts on European coastal cities: A review. *Renew. Sustain. Energy Rev.* **2023**, *184*, 113587. [\[CrossRef\]](#)
- Meerow, S.; Newell, J.P.; Stults, M. Defining urban resilience: A review. *Landsc. Urban Plan.* **2016**, *147*, 38–49. [\[CrossRef\]](#)
- Mohtat, N.; Khirfan, L. The climate justice pillars vis-à-vis urban form adaptation to climate change: A review. *Urban Clim.* **2021**, *39*, 100951. [\[CrossRef\]](#)
- Banerjee, S.; Yik, S.K.; Dzyuban, Y.; Crank, P.J.; Yi, R.P.X.; Chow, W.T. Analysing impacts of urban morphological variables and density on outdoor microclimate for tropical cities: A review and a framework proposal for future research directions. *Build. Environ.* **2022**, *225*, 109646. [\[CrossRef\]](#)
- Yang, S.; Wang, L.; Stathopoulos, T.; Marey, A.M. Urban microclimate and its impact on built environment—A review. *Build. Environ.* **2023**, *238*, 110334. [\[CrossRef\]](#)
- Laino, E.; Iglesias, G. Scientometric review of climate-change extreme impacts on coastal cities. *Ocean Coast. Manag.* **2023**, *242*, 106709. [\[CrossRef\]](#)
- Ishugah, T.F.; Li, Y.; Wang, R.Z.; Kiplagat, J.K. Advances in wind energy resource exploitation in urban environment: A review. *Renew. Sustain. Energy Rev.* **2014**, *37*, 613–626. [\[CrossRef\]](#)
- He, Q.; Silliman, B.R. Climate Change, Human Impacts, and Coastal Ecosystems in the Anthropocene. *Curr. Biol.* **2019**, *29*, R1021–R1035. [\[CrossRef\]](#) [\[PubMed\]](#)
- Xiao, L.; Wang, J.; Dong, Y.; Wu, J. Combined forecasting models for wind energy forecasting: A case study in China. *Renew. Sustain. Energy Rev.* **2015**, *44*, 271–288. [\[CrossRef\]](#)
- Guo, F.; Zhao, J.; Zhang, H.; Dong, J.; Zhu, P.; Lau, S.S.Y. Effects of urban form on sea cooling capacity under the heatwave. *Sustain. Cities Soc.* **2023**, *88*, 104271. [\[CrossRef\]](#)

20. Ma, T.; Chen, T. Outdoor ventilation evaluation and optimization based on spatial morphology analysis in Macau. *Urban Clim.* **2022**, *46*, 101335. [[CrossRef](#)]
21. Zheng, Y.; Li, W.; Fang, C.; Feng, B.; Zhong, Q.; Zhang, D. Investigating the Impact of Weather Conditions on Urban Heat Island Development in the Subtropical City of Hong Kong. *Atmosphere* **2023**, *14*, 257. [[CrossRef](#)]
22. Guo, F.; Zhang, H.; Fan, Y.; Zhu, P.; Wang, S.; Lu, X.; Jin, Y. Detection and evaluation of a ventilation path in a mountainous city for a sea breeze: The case of Dalian. *Build. Environ.* **2018**, *145*, 177–195. [[CrossRef](#)]
23. Yan, X.; Liu, Y.; Xu, Y.; Jia, M. Multistep forecasting for diurnal wind speed based on hybrid deep learning model with improved singular spectrum decomposition. *Energy Convers. Manag.* **2020**, *225*, 113456. [[CrossRef](#)]
24. Kabošová, L.; Katunský, D.; Kmet, S. Wind-Based Parametric Design in the Changing Climate. *Appl. Sci.* **2020**, *10*, 8603. [[CrossRef](#)]
25. Jalali, S.M.J.; Ahmadian, S.; Khodayar, M.; Khosravi, A.; Ghasemi, V.; Shafie-Khah, M.; Nahavandi, S.; Catalão, J.P.S. Towards novel deep neuroevolution models: Chaotic levy grasshopper optimization for short-term wind speed forecasting. *Eng. Comput.* **2022**, *38*, 1787–1811. [[CrossRef](#)]
26. Matzarakis, A.; Rutz, F.; Mayer, H. Modelling radiation fluxes in simple and complex environments—Application of the RayMan model. *Int. J. Biometeorol.* **2007**, *51*, 323–334. [[CrossRef](#)]
27. Höppe, P. The physiological equivalent temperature—A universal index for the biometeorological assessment of the thermal environment. *Int. J. Biometeorol.* **1999**, *43*, 71–75. [[CrossRef](#)] [[PubMed](#)]
28. Matzarakis, A.; Mayer, H.; Iziomon, M.G. Applications of a universal thermal index: Physiological equivalent temperature. *Int. J. Biometeorol.* **1999**, *43*, 76–84. [[CrossRef](#)]
29. Blazejczyk, K.; Epstein, Y.; Jendritzky, G.; Staiger, H.; Tinz, B. Comparison of UTCI to selected thermal indices. *Int. J. Biometeorol.* **2012**, *56*, 515–535. [[CrossRef](#)]
30. Jendritzky, G.; de Dear, R.; Havenith, G. UTCI—Why another thermal index? *Int. J. Biometeorol.* **2012**, *56*, 421–428. [[CrossRef](#)]
31. Yang, L.; Yan, H.; Lam, J.C. Thermal comfort and building energy consumption implications—A review. *Appl. Energy* **2014**, *115*, 164–173. [[CrossRef](#)]
32. Binarti, F.; Koerniawan, M.D.; Triyadi, S.; Utami, S.S.; Matzarakis, A. A review of outdoor thermal comfort indices and neutral ranges for hot-humid regions. *Urban Clim.* **2020**, *31*, 100531. [[CrossRef](#)]
33. Mayer, H.; Höppe, P. Thermal comfort of man in different urban environments. *Theor. Appl. Climatol.* **1987**, *38*, 43–49. [[CrossRef](#)]
34. Perini, K.; Chokhachian, A.; Dong, S.; Auer, T. Modeling and simulating urban outdoor comfort: Coupling ENVI-Met and TRNSYS by grasshopper. *Energy Build.* **2017**, *152*, 373–384. [[CrossRef](#)]
35. Kamel, T.M. A new comprehensive workflow for modelling outdoor thermal comfort in Egypt. *Sol. Energy* **2021**, *225*, 162–172. [[CrossRef](#)]
36. Ibrahim, Y.; Kershaw, T.; Shepherd, P.; Elkady, H. Multi-objective optimisation of urban courtyard blocks in hot arid zones. *Sol. Energy* **2022**, *240*, 104–120. [[CrossRef](#)]
37. Huang, Z.; Gou, Z.; Cheng, B. An investigation of outdoor thermal environments with different ground surfaces in the hot summer-cold winter climate region. *J. Build. Eng.* **2020**, *27*, 100994. [[CrossRef](#)]
38. Shi, Z.; Fonseca, J.A.; Schlueter, A. A parametric method using vernacular urban block typologies for investigating interactions between solar energy use and urban design. *Renew. Energy* **2021**, *165*, 823–841. [[CrossRef](#)]
39. Hamdan, D.M.A.; de Oliveira, F.L. The impact of urban design elements on microclimate in hot arid climatic conditions: Al Ain City, UAE. *Energy Build.* **2019**, *200*, 86–103. [[CrossRef](#)]
40. Bajšanski, I.V.; Milošević, D.D.; Savić, S.M. Evaluation and improvement of outdoor thermal comfort in urban areas on extreme temperature days: Applications of automatic algorithms. *Build. Environ.* **2015**, *94*, 632–643. [[CrossRef](#)]
41. Milošević, D.D.; Bajšanski, I.V.; Savić, S.M. Influence of changing trees locations on thermal comfort on street parking lot and footways. *Urban For. Urban Green.* **2017**, *23*, 113–124. [[CrossRef](#)]
42. Sung, W.; Jeong, Y. Site planning automation of apartment complex through grid-based calculation in grasshopper. *Autom. Constr.* **2022**, *138*, 104216. [[CrossRef](#)]
43. Yu, Z.J.; Yang, B.; Zhu, N.; Olofsson, T.; Zhang, G. Utility of cooling overshoot for energy efficient thermal comfort in temporarily occupied space. *Build. Environ.* **2016**, *109*, 199–207. [[CrossRef](#)]
44. Jacobsen, N.G.; Fuhrman, D.R.; Fredsøe, J. A wave generation toolbox for the open-source CFD library: OpenFoam®. *Int. J. Numer. Methods Fluids* **2012**, *70*, 1073–1088. [[CrossRef](#)]
45. Jasak, H. OpenFOAM: Open source CFD in research and industry. *Int. J. Nav. Arch. Ocean Eng.* **2009**, *1*, 89–94. [[CrossRef](#)]
46. Kabošová, L.; Chronis, A.; Galanos, T.; Kmet, S.; Katunský, D. Shape optimization during design for improving outdoor wind comfort and solar radiation in cities. *Build. Environ.* **2022**, *226*, 109668. [[CrossRef](#)]
47. Du, Y.; Mak, C.M.; Liu, J.; Xia, Q.; Niu, J.; Kwok, K. Effects of lift-up design on pedestrian level wind comfort in different building configurations under three wind directions. *Build. Environ.* **2017**, *117*, 84–99. [[CrossRef](#)]
48. Yuan, C.; Ng, E.; Norford, L.K. Improving air quality in high-density cities by understanding the relationship between air pollutant dispersion and urban morphologies. *Build. Environ.* **2014**, *71*, 245–258. [[CrossRef](#)]
49. Richards, P.J.; Hoxey, R.P. Appropriate boundary conditions for computational wind engineering models using the k-ε turbulence model. *J. Wind. Eng. Ind. Aerodyn* **1993**, *46–47*, 145–153. [[CrossRef](#)]
50. Hammond, D.S.; Chapman, L.; Thornes, J.E. Roughness length estimation along road transects using airborne LIDAR data. *Meteorol. Appl.* **2012**, *19*, 420–426. [[CrossRef](#)]

51. Xu, X.; Wu, Y.; Wang, W.; Hong, T.; Xu, N. Performance-driven optimization of urban open space configuration in the cold-winter and hot-summer region of China. *Build. Simul.* **2019**, *12*, 411–424. [[CrossRef](#)]
52. Feng, W.; Chen, J.; Yang, Y.; Gao, W.; Xing, H.; Yu, S. Multi-objective optimization of morphology for high-rise residential cluster with the regards to energy use and microclimate. *Energy Build.* **2024**, *319*, 114534. [[CrossRef](#)]
53. Gou, S.; Nik, V.M.; Scartezzini, J.; Zhao, Q.; Li, Z. Passive design optimization of newly-built residential buildings in Shanghai for improving indoor thermal comfort while reducing building energy demand. *Energy Build.* **2018**, *169*, 484–506. [[CrossRef](#)]
54. Liu, H.; Yan, F.; Tian, H. Towards low-carbon cities: Patch-based multi-objective optimization of land use allocation using an improved non-dominated sorting genetic algorithm-II. *Ecol. Indic.* **2022**, *134*, 108455. [[CrossRef](#)]
55. Ribau, J.P.; Sousa, J.M.C.; Silva, C.M. Reducing the carbon footprint of urban bus fleets using multi-objective optimization. *Energy* **2015**, *93*, 1089–1104. [[CrossRef](#)]
56. Wu, Y.; Zhan, Q.; Quan, S.J.; Fan, Y.; Yang, Y. A surrogate-assisted optimization framework for microclimate-sensitive urban design practice. *Build. Environ.* **2021**, *195*, 107661. [[CrossRef](#)]
57. Yao, Y.; Peng, Z.; Xiao, B. Parallel Hyper-Heuristic Algorithm for Multi-Objective Route Planning in a Smart City. *IEEE Trans. Veh. Technol.* **2018**, *67*, 10307–10318. [[CrossRef](#)]
58. Hakimazari, M.; Baghoolizadeh, M.; Sajadi, S.M.; Kheiri, P.; Moghaddam, M.Y.; Rostamzadeh-Renani, M.; Rostamzadeh-Renani, R.; Hamooleh, M.B. Multi-objective optimization of daylight illuminance indicators and energy usage intensity for office space in Tehran by genetic algorithm. *Energy Rep.* **2024**, *11*, 3283–3306. [[CrossRef](#)]
59. Valiyappurakkal, V.K.; Shabarise, Y.; Natawadkar, K.; Misra, K. A methodology to assess the constructibility of free-form buildings using building and surface performance indicators: Application to a case study. *Energy Build.* **2022**, *270*, 112303. [[CrossRef](#)]
60. Zhao, J.; Guo, F.; Zhang, H.; Dong, J. Mechanisms of non-stationary influence of urban form on the diurnal thermal environment based on machine learning and MGWR analysis. *Sustain. Cities Soc.* **2024**, *101*, 105194. [[CrossRef](#)]
61. Chow, W.K.; Wong, L.T. Experimental Studies on the Air Flow Characteristics Induced by a High Sidewall Grill in a Climate Chamber. *Indoor Built Environ.* **1996**, *5*, 82–98. [[CrossRef](#)]
62. Liu, K.; Xu, X.; Huang, W.; Zhang, R.; Kong, L.; Wang, X. A multi-objective optimization framework for designing urban block forms considering daylight, energy consumption, and photovoltaic energy potential. *Build. Environ.* **2023**, *242*, 110585. [[CrossRef](#)]
63. Wang, S.; Yi, Y.K.; Liu, N. Multi-objective optimization (MOO) for high-rise residential buildings' layout centered on daylight, visual, and outdoor thermal metrics in China. *Build. Environ.* **2021**, *205*, 108263. [[CrossRef](#)]
64. Zhang, J.; Liu, N.; Wang, S. Generative design and performance optimization of residential buildings based on parametric algorithm. *Energy Build.* **2021**, *244*, 111033. [[CrossRef](#)]
65. Dong, J.; Guo, R.; Lin, M.; Guo, F.; Zheng, X. Multi-objective optimization of green roof spatial layout in high-density urban areas—A case study of Xiamen Island, China. *Sustain. Cities Soc.* **2024**, *115*, 105827. [[CrossRef](#)]

Disclaimer/Publisher's Note: The statements, opinions and data contained in all publications are solely those of the individual author(s) and contributor(s) and not of MDPI and/or the editor(s). MDPI and/or the editor(s) disclaim responsibility for any injury to people or property resulting from any ideas, methods, instructions or products referred to in the content.